

1 **The impacts of regional shipping emissions on the chemical characteristics of coastal**
2 **submicron aerosols near Houston, TX**

3 Benjamin C. Schulze¹, Henry W. Wallace^{1,†}, Alexander T. Bui¹, James H. Flynn², Matt H.
4 Erickson^{2,*}, Sergio Alvarez², Qili Dai³, Sascha Usenko⁴, Rebecca J. Sheesley⁴, Robert J.
5 Griffin^{1,5}

6 ¹Department of Civil and Environmental Engineering, Rice University, Houston, TX, 77005

7 ²Department of Earth and Atmospheric Sciences, University of Houston, Houston, TX, 77204

8 ³State Environmental Protection Key Laboratory of Urban Ambient Air Particulate Matter Pollution
9 Prevention and Control, College of Environmental Science and Engineering, Nankai University, Tianjin
10 300071, China

11 ⁴Department of Environmental Science, Baylor University, Waco, TX, 76798

12 ⁵Department of Chemical and Biomolecular Engineering, Rice University, Houston, TX, 77005

13 [†]Now at Washington State Department of Ecology, Lacey WA, 98503

14 ^{*}Now at TerraGraphics Environmental Engineering, Inc., Pasco, WA, 99301

15

16 **Abstract**

17 The air quality of the Texas Gulf Coast region historically has been influenced heavily by
18 regional shipping emissions. However, the effects of the recently established North American
19 Emissions Control Area on aerosol concentrations and properties in this region are presently
20 unknown. In order to better understand the current sources and processing mechanisms
21 influencing coastal aerosol near Houston, a high-resolution time-of-flight aerosol mass

22 spectrometer (HR-ToF-AMS) was deployed for three weeks at a coastal location during May-
23 June 2016. Total mass loadings of organic and inorganic non-refractory aerosol components
24 during onshore flow periods were similar to those published before establishment of the
25 regulations. Based on estimated methanesulfonic acid (MSA) mass loadings and published
26 biogenic MSA to non-sea-salt-sulfate (nss-SO₄) ratios, an average of over 75% of the observed
27 nss-SO₄ was from anthropogenic sources, predominantly shipping emissions. Mass spectral
28 analysis indicated that for periods with similar backward-trajectory-averaged meteorological
29 conditions, air masses influenced by shipping emissions had an increased mass fraction of ions
30 related to carboxylic acids and larger oxygen-to-carbon ratios than those that avoided shipping
31 lanes, suggesting that shipping emissions increase marine organic aerosol (OA) oxidation state.
32 Amine fragment mass loadings were correlated positively with anthropogenic nss-SO₄ during
33 onshore flow, implying anthropogenic-biogenic interaction in marine OA production. Model
34 calculations also suggest that advection of shipping-derived aerosol may enhance inland
35 aqueous-phase secondary OA production. These results imply a continuing role of shipping
36 emissions on aerosol properties over the Gulf of Mexico and suggest that further regulation of
37 shipping fuel sulfur content will reduce coastal submicron aerosol mass loadings near Houston.

38

39 **1. Introduction**

40 Seaborne trade is a relatively inexpensive and efficient mechanism to transport goods across
41 the globe (IMO, 2012). As a result, such transportation is thought to account for more than 90%
42 of global trade volume (Eyring et al., 2010; IMO, 2012) and has been growing rapidly in the past
43 two decades (Lack et al., 2009; Eyring et al., 2010; Tournadre, 2014; Johansson et al., 2017). As
44 large commercial shipping vessels historically have had little or inconsistent regulation in

45 international waters, they frequently burn low-quality residual fuel oils, leading to considerable
46 emissions of sulfur dioxide (SO₂), nitrogen oxides (NO_x), and particulate matter (PM) (Lack et
47 al., 2009; Murphy et al., 2009; Czech et al., 2017). Recently, increasing attention has been paid
48 to the impact of these emissions on ambient PM mass loadings in coastal areas, with notable
49 contributions in Europe (Viana et al., 2014 and references therein; Aksoyoglu et al., 2016), Asia
50 (Zhao et al., 2012; Liu et al., 2016), and the United States (Vutukuru and Dabdub, 2008;
51 Agrawal et al., 2009). Coastal populations exposed to these emissions are subsequently affected
52 by numerous negative health impacts. Corbett et al. (2007) estimated that shipping activity was
53 responsible for 60,000 global premature mortalities annually. More recent studies have
54 confirmed links between shipping emissions and increased hospitalizations (Tian et al., 2013).

55 The Port of Houston is the second largest in the United States (U.S.) by tonnage (Port of
56 Houston, 2017), and the Gulf of Mexico has a high density of marine vessel emissions relative to
57 many other marine locations (Tournadre, 2014; Johansson et al., 2017); however, relatively little
58 research has aimed to characterize the impact of shipping emissions on Houston air quality.
59 During the Texas Air Quality Study and Gulf of Mexico Atmospheric Composition and Climate
60 Study 2006, measurements onboard the R/V Brown were used to characterize aerosol sources
61 over the Gulf of Mexico (Bates et al., 2008; Russell et al., 2009). Measured submicron aerosol
62 sulfate (SO₄) mass loadings during periods of onshore flow were significantly larger than
63 expected for a marine environment, leading Bates et al. (2008) to conclude that shipping
64 emissions contributed heavily to total submicron aerosol mass. Russell et al. (2009) further
65 determined that an “oil combustion/refining” organic factor accounted for 33-68% of organic
66 aerosol (OA) mass during onshore flow periods. Using a large-scale three dimensional air quality
67 model, Caiazzo et al. (2013) calculated that in 2005, marine vessel emissions increased annual

68 average PM mass loadings across the Texas Gulf Coast by ~ 0.5 to $1 \mu\text{g m}^{-3}$, leading to 645
69 estimated premature mortalities in Texas.

70 Recent concerns over the health impacts of marine vessel emissions led to the establishment
71 of the North American Emissions Control Area (ECA; U.S. Environmental Protection Agency
72 (EPA), 2010). Prior to establishment of the ECA, multiple studies demonstrated that shipping
73 emissions of PM were related to fuel sulfur content (FSC) (Kasper et al., 2007; Lack et al., 2009
74 and references therein), leading to the requirement that shipping vessels within 200 nautical
75 miles of the U.S. and Canadian coast reduce their FSC from the commonly utilized 3-4% (by
76 mass) to only 1%. In 2015, the limit was reduced to 0.1% (Zetterdahl et al., 2017). In order to
77 comply with these regulations, marine vessels typically switch from low-grade heavy fuel oil to
78 marine gas oil or marine diesel oil at the ECA boundary; however, low-FSC residual fuels have
79 also recently become available (Wan et al., 2016; Czech et al., 2017). Numerous studies have
80 demonstrated that such fuel switching dramatically reduces emissions of SO_2 , SO_4 , primary OA
81 (POA), and black carbon (Lack et al., 2011; Browning et al., 2012; Tao et al., 2013; Zetterdahl et
82 al., 2017).

83 Using the U.S. Interagency Monitoring of Protected Visual Environments network and
84 positive matrix factorization (PMF) modeling, Kotchenruther (2016) determined that the average
85 decrease in annual $\text{PM}_{2.5}$ (that with diameters less than or equal to $2.5 \mu\text{m}$) from residual fuel
86 combustion (i.e., shipping emissions) in U.S. coastal locations due to establishment of the ECA
87 (i.e., pre-2012 to 2016) was 74.1%. However, at two sites along the Gulf Coast (located in
88 Louisiana and Florida), the average reduction was only 35-50% (Kotchenruther, 2016). While
89 the reason for the difference between the Gulf sites and the rest of the country is currently
90 unclear, it is nevertheless evident that the implementation of the ECA may have drastically

91 changed the speciation and total mass loading of aerosol over the Gulf of Mexico, presenting the
92 need for further research on this source.

93 Shipping emissions also may have numerous secondary effects on marine aerosol. Models
94 indicate that shipping-related NO_x emissions likely elevate hydroxyl radical (OH) concentrations
95 within the marine boundary layer (MBL) (Chen et al., 2005; Kim et al., 2009; Kim et al., 2013),
96 potentially impacting the oxidation state of marine OA. Furthermore, production of the two most
97 commonly identified components of marine secondary OA (SOA), methanesulfonic acid (MSA)
98 and dimethyl/diethylamines (Facchini et al., 2008; Claeys et al., 2009; Rinaldi et al., 2010), may
99 be enhanced in the presence of shipping emissions (Gaston et al., 2010; Sorooshian et al.,
100 2015a). Finally, shipping-related SO₄ should increase submicron mass loadings of aerosol liquid
101 water (ALW), which may subsequently impact aqueous processing of water-soluble organics
102 (Carlton and Turpin, 2013). These effects are difficult to model on a global scale due to the
103 complexities of accurately simulating the photochemistry and physical transport of shipping
104 plumes (Kim et al., 2009), making field measurements useful to evaluate these hypotheses.

105 In the present study, three weeks of coastal air measurements were performed near Houston,
106 TX, to investigate the impact of marine vessel emissions on ambient aerosol mass and
107 composition. Specific focus was placed on apportioning anthropogenic and biogenic sources of
108 SO₄, attributing anthropogenic SO₄ to marine vessel emissions, investigating links between
109 marine vessel emissions and measured OA, and exploring whether these emissions appear to
110 influence OA composition, amine/MSA aerosol formation, or ALW.

111 **2. Experimental Methods**

112 **2.1 Sampling Site Characterization**

113 Atmospheric measurements were conducted May 24 - June 14, 2016, at a private coastal
114 home southwest of Galveston, Texas (29.074°N, 95.125°W). Figure 1 presents an overview of
115 the sampling location. The site is approximately 75 km directly south of the Houston Ship
116 Channel (HSC) and is therefore a similar distance from Houston's urban core. In addition, the
117 primary inlet to Galveston Bay used for commercial shipping is about 45 km to the northeast.
118 The nearest road, Highway 257 just north of the site, connects the cities of Galveston and
119 Freeport, TX, and receives relatively little traffic. As a result, this location is likely to be less
120 influenced by primary anthropogenic emissions than recent campaigns in Houston that took
121 place closer to the urban core (Cleveland et al., 2012; Bean et al., 2016; Leong et al., 2017;
122 Wallace et al., 2018). Instruments including a high-resolution time-of-flight aerosol mass
123 spectrometer (HR-ToF-AMS, Aerodyne, Inc.) and those measuring traces gases and
124 meteorological parameters were housed inside the University of Houston/Rice University Mobile
125 Air Quality Laboratory (MAQL), which was stationed outside of the private home and has been
126 described previously (Leong et al., 2017). As measurements were performed during a single
127 three-week period, presented results should be viewed with this limitation in mind. Ultimately,
128 longer time-frame studies are warranted to test whether results presented here are consistently
129 observed.

130 **2.2 HR-ToF-AMS Operation**

131 The chemical composition of non-refractory submicron PM (NR-PM₁) was determined
132 through the use of a HR-ToF-AMS (DeCarlo et al., 2006). Numerous detailed descriptions of
133 HR-ToF-AMS operation can be found elsewhere (DeCarlo et al., 2006; Canagaratna et al.,
134 2007). Air flow was drawn into the HR-ToF-AMS through a 2.5- μ m cut diameter Teflon®-
135 coated cyclone located on top of the MAQL mast approximately 6 m above ground level.

136 Incoming air is transmitted through a 100- μm critical orifice, after which particles are focused
137 into a beam through the use of an aerodynamic lens and accelerated under high vacuum (10^{-5}
138 Torr) into the sizing chamber. After passing the sizing chamber, non-refractory chemical
139 components are flash vaporized at approximately 600°C and ionized at 70 eV. Ionized mass
140 fragments are then directed into the time-of-flight mass spectral detection region. For this study,
141 the HR-ToF-AMS was operated in V-mode (higher signal, less mass-to-charge (m/z) resolution
142 compared to the alternative W-mode), and data were collected over 80-s intervals. A nafion dryer
143 was placed upstream of the HR-ToF-AMS inlet to maintain a sampling line relative humidity
144 (RH) below 40%.

145 **2.3 HR-ToF-AMS Data Analysis**

146 The HR-ToF-AMS data were analyzed with the SQUIRREL v 1.57I and PiKA v 1.16I
147 (D. Sueper, University of Colorado-Boulder) software packages within Igor Pro (Wavemetrics,
148 Inc.). The collection efficiency (CE) of the HR-ToF-AMS, which is influenced by sampling line
149 RH as well as particle composition, was determined using the composition-dependent calculator
150 within the SQUIRREL and PiKA software packages (Middlebrook et al., 2011). This method
151 produced a CE of 0.5 for the majority of the campaign (89% of the time). High-resolution
152 analysis was performed on each ion in the m/z range 10-125, and elemental analysis of organic
153 composition was performed using the Improved-Ambient method (Canagaratna et al., 2015). The
154 ionization efficiency of the HR-ToF-AMS with respect to nitrate (NO_3) was calibrated before
155 and after the campaign using 350-nm ammonium nitrate (NH_4NO_3) particles following standard
156 procedures. In order to calculate campaign-averaged detection limits, filtered air was sampled
157 every two days for approximately 30 minutes at a time, and the detection limit was calculated as

158 three times the standard deviation of the filter measurements. Detection limits are provided in
159 Table S1 in the supplemental information (SI).

160 **2.4 Positive Matrix Factorization**

161 Positive matrix factorization analysis (Paatero and Tapper, 1994) was performed on the
162 high-resolution HR-ToF-AMS mass spectral dataset in order to further investigate potential
163 sources and transformation processes of measured OA. The PMF technique has been applied
164 extensively in urban (Ulbrich et al., 2009; Ng et al., 2010), rural/downwind (Crippa et al., 2014
165 and references therein), and coastal locations (Hildebrandt et al., 2010; Hildebrandt et al., 2011;
166 Schmale et al., 2013) to characterize classes of compounds that constitute OA. The PMF model
167 assumes that the time series of organic mass spectra can be divided into a number of temporally
168 unvarying components. These components, defined by their fixed mass spectra, contribute
169 varying amounts of organic mass to the total organic signal at each time. Details on PMF and
170 the resulting factors are included in the SI.

171 **2.5 HYSPLIT Backward Trajectory Calculation**

172 Analysis of air mass history is often a useful tool for characterizing likely sources and
173 processes affecting measured aerosol composition. As a result, 120-hr backward trajectories
174 were calculated at heights of 100, 200, 300, 400, and 500 m using the Hybrid Single-Particle
175 Lagrangian Integrated Trajectory (HYSPLIT) model (Draxler and Rolph, 2003) for every hour
176 during the campaign. Meteorological data at a resolution of 12 km x 12 km were obtained from
177 the North American Mesoscale Forecast System (NAMS) archive
178 (<https://ready.arl.noaa.gov/archives.php>) through the HYSPLIT software. Recorded
179 meteorological parameters such as solar flux (W/m^2), mixing layer depth, and precipitation were

180 averaged for each trajectory to provide insight into influences of photochemistry, mixing, and
181 possible wet deposition during transport. In addition, the overall length of each five-day
182 trajectory was used to represent an average wind speed, as knowledge of historical wind speed is
183 important for predictions concerning the influence of POA particles in ocean environments (Zorn
184 et al., 2008; Russell et al., 2010; Ovadnevaite et al., 2011).

185 **2.6 Weighted Potential Source Contribution Function**

186 In order to provide further insight into likely aerosol source regions during the campaign,
187 the weighted potential source contribution function (WPSCF) was applied to the dataset. The
188 WPSCF combines measured mass loadings of atmospheric species with air mass trajectories to
189 determine probable source locations. The WPSCF method has been used to study regional
190 sources of air pollutants at different receptor sites (Hopke et al., 1995; Zhu et al., 2011; Guo et
191 al., 2014). For this study, the WPSCF analysis utilized HYSPLIT trajectories described
192 previously. The spatial area covered by the trajectories was divided into a grid of $0.5^\circ \times 0.5^\circ$
193 cells, and the number of trajectory segment endpoints located in each cell for five different
194 starting heights (100, 200, 300, 400, and 500 m) was determined. Incorporation of multiple
195 starting heights accounts for the general clockwise rotation of air mass backward trajectories
196 with altitude. While these cell sizes are relatively small (typical values $\sim 0.5^\circ$ - 2°), this study was
197 particularly focused on attribution of measured SO_4 to specific locations within the Gulf of
198 Mexico (i.e., shipping lanes), which requires a small cell size.

199 In order to calculate the WPSCF value for each cell, the total potential source
200 contribution function (TPSCF) value is first calculated and then weighted. The value of the
201 TPSCF function for a specific grid cell (i, j) is calculated using (Hopke et al., 1995; Guo et al.,
202 2014):

203
$$TPSCF_{i,j} = \frac{\sum m_{i,j}^k}{\sum n_{i,j}^k} \quad (1)$$

204 where $n_{i,j}^k$ represents the total number of trajectory segment endpoints located within cell i,j for
 205 height k , while $m_{i,j}^k$ represents the number of these endpoints that also correspond to measured
 206 values of a specific species above a critical value, in this case the 75th percentile (Hopke et al.,
 207 1995; Guo et al., 2014).

208 In the case of highly variable air mass trajectories or strong local sources during a campaign,
 209 distant grid cells that were intersected by only a small number of trajectories may be incorrectly
 210 assumed to represent likely sources. To prevent this, a weighting function is applied to TPSCF
 211 values based on the $n_{i,j}^k$ value, with higher weight given to cells that were intersected by more
 212 trajectories. The weighting method, based on the power of the number of trajectories at a specific
 213 height, is (Guo et al., 2014)

214
$$W(\sum n_{i,j}^k) = \begin{cases} 1, & T^{0.7} < \sum n_{i,j}^k \\ 0.7, & T^{0.56} < \sum n_{i,j}^k \leq T^{0.7} \\ 0.42, & T^{0.42} < \sum n_{i,j}^k \leq T^{0.56} \\ 0.17, & \sum n_{i,j}^k \leq T^{0.42} \end{cases} \quad (2)$$

215 where T represents the total number of trajectories calculated at each specific height. The
 216 WPSCF value is then calculated by applying the relevant weights to each cell.

217
$$WPSCF_{i,j} = W_{i,j} \times TPSCF_{i,j} \quad (3)$$

218 **2.7 MSA Calibration**

219 Methanesulfonic acid is widely regarded as a robust indicator of SOA production from
 220 marine sources (Facchini et al., 2008; Crippa et al., 2013; Schmale et al., 2013; Ovadnevaite et

221 al., 2014). In addition, MSA is often the most abundant identifiable component of marine OA
222 (Facchini et al., 2008; Claeys et al., 2009). Recent work has identified that MSA mass loadings
223 can be quantified in near-real time by the HR-ToF-AMS provided that accurate instrument-
224 specific calibrations are performed (Zorn et al., 2008; Ovadenvaite et al., 2014; Huang et al.,
225 2017). As MSA fragments into both organic and inorganic SO_4 -containing ions within the HR-
226 ToF-AMS, accurate mass prediction requires reconstruction of the compound based on
227 knowledge of the fragmentation pattern in the specific instrument being used (Zorn et al., 2008).
228 As such, calibrations were performed following the procedure of Ovadnevaite et al. (2014).

229 A 0.02% aqueous solution of MSA (Sigma-Aldrich, >99.0% purity) was nebulized by a
230 TSI, Inc. atomizer (model 3076) and passed through a differential mobility analyzer (BMI, Inc.)
231 to size select particles 300-nm in mobility diameter. These particles were then measured by the
232 HR-ToF-AMS. Mass spectra from two separate calibrations are provided in Figure S13. While
233 MSA fragments into a variety of ions within the HR-ToF-AMS (CH_3^+ , CHS^+ , CH_3SO_2^+ , SO^+ ,
234 SO_2^+ , etc.), the CH_3SO_2^+ ion is thought to originate almost exclusively from MSA, as other
235 organosulfate standards measured by the HR-ToF-AMS show negligible contributions to
236 CH_3SO_2^+ (Huang et al., 2015). Therefore, MSA mass loadings during the campaign were
237 calculated based on the ratio of this ion to the total MSA mass measured during the calibrations
238 (Huang et al., 2015; Huang et al., 2017). The average ratio measured during the two calibrations
239 (18.18), was similar to that determined from the calibration of Huang et al. (2017) (23.81).

240 **2.8 Distinction Between Anthropogenic and Biogenic nss-SO₄**

241 The MSA measurements also allow estimation of the relative contributions of biogenic and
242 anthropogenic (primarily due to shipping) sources of non-sea-salt (nss)-SO₄ in marine
243 environments. In many studies attempting to apportion the impact of shipping emissions on

244 measured aerosol mass, ratios of trace metals specific to heavy fuel oil combustion are used as
245 tracers (Zhao et al., 2012; Viana et al., 2014; Kotchenruther, 2016). However, in cases where
246 such data are unavailable, biogenic sulfur sources, based on the oxidation chemistry of dimethyl
247 sulfide (DMS), should produce a latitude-specific biogenic MSA/nss-SO₄ ratio, presenting a
248 metric to apportion biogenic and anthropogenic nss-SO₄ (Jung et al., 2014). Specifically, DMS
249 oxidation, which primarily occurs through initial reaction with OH, can either proceed through
250 an abstraction or addition pathway (Hynes et al., 1986). The addition pathway, which is favored
251 at lower temperatures prevalent at higher latitudes, mainly produces dimethylsulfoxide and
252 MSA. The abstraction pathway, favored in higher temperatures, primarily produces SO₂ and
253 therefore eventually nss-SO₄ (Hynes et al., 1986; Jung et al., 2014). As a result, previous long
254 distance remote trans-oceanic cruises have observed significant latitudinal gradients in the
255 MSA/nss-SO₄ ratio in both the Atlantic and Pacific Oceans (Jung et al., 2014; Huang et al.,
256 2017), with consistently larger values at high latitudes.

257 As nss-SO₄ measured in marine environments is often produced by a combination of
258 anthropogenic and biogenic sources, multiple linear regression (MLR) analysis is often used to
259 extract the biogenic MSA/nss-SO₄ ratio from ambient marine aerosol data. The MLR technique
260 assumes that marine nss-SO₄ is produced from a biogenic source, which can be traced with MSA
261 mass loadings (used as one predictor variable), and an anthropogenic source, which can be traced
262 using concentrations of heavy metals emitted by shipping vessels (e.g., antimony) (used as the
263 second predictor variable) (Savoie et al., 2002). Previously published agreement between
264 measured and predicted nss-SO₄ using the MLR method was robust ($R^2 > 0.7$) (Savoie et al.,
265 2002). For this study, the biogenic MSA/nss-SO₄ ratio (0.053) determined by Savoie et al. (2002)
266 using multiple linear regression (MLR) at Bermuda was utilized to apportion biogenic versus

267 anthropogenic sources of nss-SO₄, as Bermuda is the closest location to our sampling site in
268 terms of latitude (32°N at Bermuda versus 29°N at our sampling site). In addition to being
269 collected at the closest location to our sampling site, the ratio extracted at Bermuda is the lowest
270 reported ratio in the literature, to the authors' knowledge. A more recent study by Lin et al.
271 (2012) quantified the biogenic MSA/nss-SO₄ ratio of submicron marine aerosol using sulfur
272 isotopic data at varying latitudes across the Atlantic Ocean. The authors reported ratios similar to
273 or larger than 0.053 at all sampled latitudes. As a result, the application of other published ratios
274 will only increase the fraction of nss-SO₄ attributed to anthropogenic sources.

275 However, as the biogenic MSA/nss-SO₄ ratio was originally determined using samples of
276 total suspended particulate matter (i.e., no size-cutoff) application of the ratio to PM₁ data should
277 produce an upper-limit estimate of the anthropogenic fraction of marine nss-SO₄. Briefly, as
278 previous field and laboratory studies have noted that MSA solubility decreases with solution
279 acidity (Kerminen et al., 1997; Jung et al., 2014), the presence of acidic sulfate aerosol can shift
280 the size distribution of MSA towards larger, more alkaline particles relative to sulfate (a stronger
281 acid) (Jung et al., 2014). This effect, if substantial, could cause the HR-ToF-AMS to report a
282 lower observed MSA/nss-SO₄ ratio than would be observed by an instrument measuring both
283 submicron and super-micron PM. However, Saltzman et al. (1983) found that the size
284 distributions of MSA and SO₄ measured in the Gulf of Mexico were quite similar, with around
285 75% of MSA and approximately 87% of nss-SO₄ contained within submicron particles,
286 suggesting that the overall uncertainty resulting from this effect is small.

287 Quantification of anthropogenic nss-SO₄ also requires that the contribution of sea salt
288 (ss)-SO₄ be determined. Using laboratory calibrations, the ss-SO₄ mass loading measured by the
289 HR-ToF-AMS when sampling a sea-salt standard (Lake Products Co., ASTM D1141), is

290 approximately $26 \pm 2\%$ of the corresponding chloride mass loading. Using this ratio and
291 measured chloride mass loadings during the campaign, ss-SO_4 contributed only $0.4 \pm 0.4\%$ of the
292 total SO_4 mass loading. Therefore, to produce an estimate of anthropogenic nss-SO_4 , the HR-
293 ToF-AMS estimate of MSA is divided by the biogenic MSA/ nss-SO_4 ratio published by Savoie
294 et al. (2002) to produce a “biogenic” mass loading of nss-SO_4 . This amount is subtracted from
295 the total nss-SO_4 measured by the HR-ToF-AMS, and the remaining nss-SO_4 is assumed to be
296 anthropogenic. This technique could lead to under-prediction of sea-salt sulfate mass loadings in
297 the case of substantial chloride displacement by nitrate in the marine boundary layer. However,
298 the near-detection limit concentrations of nitrate measured during the marine period of the study
299 ($0.02 \pm 0.01 \mu\text{g m}^{-3}$) suggests that this possibility has at most a negligible influence of our results.
300 Multiple lines of evidence described in Section 3.2 support the use of this technique.

301 **2.9 Ancillary Measurements**

302 A variety of trace gases and meteorological parameters were measured during the campaign.
303 All trace gas and meteorological data were measured with a 5-minute averaging time. Individual
304 NO_x species (nitric oxide and nitrogen dioxide (NO_2)) and total reactive gas-phase nitrogen were
305 measured using high sensitivity chemiluminescence monitors (AQD, Inc.). Ozone (O_3) mixing
306 ratios were measured with an ultraviolet absorption instrument (2BTech, Inc., model 205), and
307 carbon monoxide mixing ratios were measured using high-resolution cavity enhanced direct-
308 absorption spectroscopy (Los Gatos Research, Inc.). Sulfur dioxide was measured with a pulsed
309 fluorescence analyzer (ThermoFischer Scientific, model 43i). Ambient temperature, pressure,
310 wind speed, and wind direction were measured using an RM Young meteorological station.

311 **3. Results and Discussion**

312 **3.1 Campaign Overview**

313 Figure 2 displays the speciated aerosol mass loadings, PMF factor contributions, important
314 trace gas concentrations, and meteorological conditions encountered during the campaign.
315 Overall, the average NR-PM₁ mass loading was 4.66 ± 3.17 (one standard deviation) $\mu\text{g m}^{-3}$ and
316 was dominated at times by either SO₄ (44% on average) or OA (42%). As the measurements
317 were performed in the early summer in close proximity to the coast, RH was relatively high
318 (average 81%), conditions were generally sunny, and temperatures were warm (average 27.3°C).
319 Examination of the aerosol time series data reveals three distinct period types. Marine periods
320 are characterized by consistent on-shore flow, while continental periods are characterized by off-
321 shore flow or daily land- and sea-breeze circulation patterns. A three-day period influenced by
322 the passage of two cold fronts and a low pressure (LP) system that produced heavy cloud cover,
323 intermittent rain, and a distinct aerosol diurnal profile was termed “Frontal/LP.”

324 Each of these periods contained a unique dominant PMF factor resembling low-volatility
325 oxygenated organic aerosol (OOA) (Ng et al., 2010), denoted as OOA-1, OOA-2, or OOA-3
326 (Figure 3). An overview of the average aerosol and trace gas characteristics during each period is
327 provided in Table 1, and a comparison to previous campaigns in the Houston region is shown in
328 Figure S14. While the extracted PMF factors are highlighted briefly below and summarized in
329 Table 2, more detailed factor descriptions are included in the SI.

330 The majority of the campaign (~12 days total), characterized by onshore flow conditions with
331 wind directions generally between 120° and 240°, was classified as “marine.” During these
332 periods, which encompass 5/24-6/1 and 6/10-6/14, aerosol mass loadings were relatively stable
333 from day-to-day. Interestingly, average observed mass loadings were much larger in the first
334 portion of the marine period ($4.69 \mu\text{g m}^{-3}$) (5/24-6/1) than in the second ($2.71 \mu\text{g m}^{-3}$) (6/10-
335 6/14), despite similar local wind direction, O₃, and meteorological conditions, implying that air

336 mass history has a large influence on marine aerosol loadings. The observation of SO₄ mass
337 loadings much larger than 1 μg m⁻³, which is generally the maximum observed in remote marine
338 locations, even during periods of high biological activity (Zorn et al., 2008; Rinaldi et al., 2010;
339 Schmale et al., 2013; Ovadnevaite et al., 2014), supports either a major anthropogenic aerosol
340 source in the Gulf of Mexico or an influence from continental recirculation; however, backward
341 trajectory analysis combined with an investigation of relevant source magnitudes, described in
342 Section 3.3, points to a marine anthropogenic source. The average mass loading of SO₄ plus NH₄
343 (3.04 μg m⁻³) was similar to that measured during onshore flow by Bates et al. (2008) (3 μg m⁻³),
344 despite recent regulations on shipping emissions, while measured OA mass loadings were larger
345 during this study (0.72 μg m⁻³ versus 0.38 μg m⁻³ from Bates et al. (2008)). The OA, which
346 constituted 21% of total mass, was highly oxidized (average oxygen to carbon ratio, O:C = 0.73),
347 consistent with previous measurements of marine aerosols (Russell et al. 2009; Chang et al.,
348 2011; Schmale et al., 2013). The average mass fraction of m/z 44 (f₄₄), a metric used to describe
349 the extent of OA oxidation, was 0.15, a value very similar to that observed by Russell et al.
350 (2009) during marine flow conditions (0.16), suggesting that on average, the oxidation state of
351 marine OA over the Gulf of Mexico has not changed substantially since ECA implementation.
352 However, as these comparisons are based on only three to four weeks of data collected during
353 each of the two time periods, the results should be interpreted with this limitation in mind.

354 The light winds observed during the campaign suggest that little of the measured marine OA
355 was the result of organic-enriched sea spray, as this production pathway generally requires
356 significant white-cap coverage, which is typically only observed above wind speeds of 7-8 m/s
357 (Gantt et al., 2011; Shank et al., 2012; Ovadnevaite et al., 2011; Schmale et al., 2013; Frossard et
358 al., 2014). Local wind speeds were virtually never above 8 m/s (Figure 2), and 5-day averaged

359 wind speeds calculated using total trajectory lengths were only >8 m/s for 4% of the marine
360 period. Potential major sources of OA therefore include secondary production through
361 processing of biogenic volatile organic compounds (VOCs), as well as primary and secondary
362 production from shipping emissions (Lack et al., 2009; Coggon et al., 2012). This hypothesis is
363 supported by the fact that marine OA composition was dominated by a highly oxidized PMF
364 factor, OOA-3 (O:C = 0.77; 55% of OA on average) (Figure S5), that was moderately correlated
365 with SO₄ (R² = 0.55) and displayed little diurnal variation.

366 Two storms occurred during the sampling campaign. The first (5/27) caused a loss of power
367 to the HR-ToF-AMS and the data gap shown in Figure 2; the second, denoting the beginning of
368 the “Frontal/LP” period, caused a rapid reduction in aerosol mass that was followed by three
369 days of markedly different aerosol characteristics, despite initially similar wind directions.
370 Diurnal profiles of virtually all NR-PM₁ species during the frontal/LP period are distinct from
371 the preceding marine period (Figure 3) and show maximum concentrations at night. Satellite
372 images of the area show the arrival of a large-scale frontal system on 6/2 and the presence of
373 heavy cloud cover through 6/5 (Figure S15). The O:C ratio during this period is the highest of
374 the campaign, which, combined with the strong correlation between diurnal trends of OA and
375 SO₄ (R² = 0.78) suggests measured OA represents regional background OA that is diluted with
376 the rise of the boundary layer in the morning. The dominant PMF factor extracted during this
377 period (OOA-1) had an O:C ratio (1.15) similar to the most aged OA observed in urban areas
378 (Hayes et al., 2013) implying an influence of either extensive atmospheric processing during
379 transport (Ortega et al., 2016), aqueous processing of highly oxidized water soluble organics
380 (e.g., glyoxal O:C = 1) (Chhabra et al., 2010), or some combination of the two.

381 The third identified period, which occurred from 6/6-6/9, shows evidence of continentally
382 influenced air masses and a multi-day increase of NR-PM₁ following passage of the frontal
383 system. The organic to SO₄ ratio shifts from a value of 0.34 during the marine period, typical of
384 marine environments (Coggon et al., 2012), to an average value of 3.08, highlighting the
385 predominance of OA sources within the Houston region. Local wind direction measured from
386 6/6-6/8 appears to show a land-sea breeze type circulation pattern, and midday O₃ concentrations
387 during this period reach the highest levels of the campaign (Figure 2). Diurnal profiles of NR-
388 PM₁ species highlight the influence of local photochemistry and/or boundary layer dynamics
389 (i.e., downward mixing of aged OA into the growing boundary layer) on aerosol mass loadings
390 (Figure 3). OOA-2, the dominant PMF factor during this period (72%), displays a diurnal profile
391 similar to a previously extracted OOA factor in Houston's urban core (Cleveland et al., 2012) but
392 is much more oxidized (O:C = 0.79 in this study versus 0.46 in Cleveland et al. (2012)),
393 highlighting the effect of aging during transport. Plotting mass loadings of OOA-2 against
394 ambient CO concentrations produces a slope of ~150 μg m⁻³/ppmv during this period. This value
395 is similar to previous aircraft measurements of aged industrial plumes in Houston (Bahreini et
396 al., 2009; Wood et al., 2010). Modeling results have suggested that biogenic VOCs contribute
397 little OA during Houston industrial plume transport (Bahreini et al., 2009) except in the case of
398 advection into the forested north of Houston (Brown et al., 2013), which suggests a likely
399 anthropogenic origin of OOA-2.

400 **3.2 Analysis of MSA Mass Loadings**

401 The time series of calculated MSA mass loadings is shown in Figure 4, as are concentrations
402 determined for the three distinct periods described previously and comparisons with literature
403 values. Overall during the marine period, MSA mass ranged from ~0 to 0.07 μg m⁻³ and showed

404 moderate correlation with nss-SO₄ ($R^2 = 0.46$) and weak correlation with OA ($R^2 = 0.12$),
405 suggesting major additional sources of both nss-SO₄ and OA over the MBL. While previous
406 MSA measurements in the Gulf of Mexico are sparse, Saltzman et al. (1983) recorded submicron
407 mass loadings of 0.022-0.066 $\mu\text{g m}^{-3}$ in Miami, in agreement with our results. In addition, our
408 results align well with previous submicron measurements taken at lower latitudes in both the
409 Atlantic and Pacific Oceans, as well as with measurements taken at higher latitudes while
410 sampling tropical air masses (Figure 4) (Zorn et al., 2008; Ovadnevaite et al., 2014; Huang et al.,
411 2017).

412 On average, MSA accounts for only 3.2% of submicron OA during marine periods, a value
413 much lower than observed in previous coastal measurements with a HR-ToF-AMS. For instance,
414 Crippa et al. (2013) reported that MSA accounted for approximately 20% of submicron OA in
415 Paris when air masses traveled from marine locations. At Mace Head, Ireland, MSA represented
416 12.5-18% of submicron OA during May and June when air masses traveled from the tropics
417 (Ovadnevaite et al., 2014). However, before establishment of the ECA, Russell et al. (2009)
418 found that during onshore flow in the Gulf of Mexico, between 52 and 89% of organic mass
419 could be attributed to oil combustion/refining and wood smoke-related sources. Therefore, the
420 small MSA mass fraction observed here is likely the result of strong remaining anthropogenic
421 OA sources over the Gulf. This hypothesis is supported by the relatively weak correlation
422 between the dominant marine PMF factor (OOA-3) and MSA ($R^2 = 0.41$). For comparison, the
423 distinctly biogenic marine PMF factor extracted by Crippa et al. (2013) in Paris correlated
424 strongly with MSA ($R^2 = 0.84$).

425 Quantification of the MSA/OA ratio permits a rough calculation of the contribution of
426 biogenic sources to total marine OA. Using an assumption that MSA should only represent 5-

427 10% of total biogenic OA under pristine conditions over the Gulf of Mexico (a low estimate
428 based on the previous observations discussed), calculation of the mass fraction of biogenic OA
429 based on this ratio (MSA/Bio. OA = 0.05-0.1) and the measured MSA/Total OA ratio
430 (MSA/Total OA = 0.032) implies biogenic sources only produce ~32-64% of total measured
431 marine OA. In addition, vanadium, an element common to shipping emissions, is thought to act
432 as a catalyst to MSA formation (Gaston et al., 2010). As oil combustion emissions were
433 responsible for a major fraction of OA over the Gulf of Mexico in the past (Russell et al., 2009),
434 this type of catalytic process may be enhancing MSA production relative to more pristine
435 locations at similar latitudes. This further suggests that the assumption that MSA accounts for
436 only 5-10% of biogenic OA is likely a low estimate.

437 MSA mass loadings were positively, though only slightly, correlated with trajectory-
438 averaged solar flux ($R^2 = 0.12$) and negatively correlated with trajectory length (i.e., wind speed)
439 ($R^2 = 0.16$). The lack of a strong correlation with these parameters is partly due to the fact that
440 DMS is emitted primarily in regions with high concentrations of biological organisms in the sea-
441 surface layer, which typically occur close to the coast. Therefore, emissions are not uniform
442 across the Gulf of Mexico (Sorooshian et al., 2009). Often, high MSA mass loadings are linked
443 to specific locations of high biological activity through analysis of backward trajectories and
444 comparison to chlorophyll-*a* levels (Sorooshian et al., 2009; Gaston et al., 2010; Schmale et al.,
445 2013; Sorooshian et al., 2015a; Huang et al., 2017). While the accuracy of satellite-derived
446 measures of chlorophyll-*a* as an indicator of DMS production potential is still under debate
447 (Sorooshian et al., 2009; Huang et al., 2017), the data here support a link between oceanic
448 chlorophyll-*a* and MSA mass loadings, as a peak in MSA mass is observed on 6/11, when

449 backward trajectory analysis indicates air masses slowly traveled over the nutrient-rich waters
450 close to the coast and near the mouth of the Rio Grande River (Figure S16).

451 **3.3. Quantifying Anthropogenic Contributions to Marine Aerosol Mass**

452 The average MSA/nss-SO₄ ratio measured during the marine period was 0.012. Applying the
453 biogenic MSA/nss-SO₄ ratio determined by Savoie et al. (2002) indicates that an average of 77%
454 of nss-SO₄ (1.8 μg m⁻³) is the result of anthropogenic sources during onshore flow (Figure 4c).
455 This value likely represents an upper limit (see Section 2.8). Furthermore, as the partitioning of
456 gaseous ammonia (NH₃) to the aerosol phase is driven by the neutralization of acidic SO₄, mass
457 loadings of nss-SO₄ and NH₄ are highly correlated during the marine period (R² = 0.97). As a
458 result, an estimate of an “anthropogenic” mass loading of NH₄ can be calculated based on the
459 NH₄/nss-SO₄ ratio and the calculated anthropogenic fraction of nss-SO₄. The classification of a
460 fraction of NH₄ as “anthropogenic” therefore refers to the necessity of an anthropogenic species
461 (in this case nss-SO₄) for the production of NH₄ aerosol, rather than anthropogenic NH₃
462 emissions. By applying this method and combining anthropogenic NH₄ and nss-SO₄ mass
463 loadings, anthropogenic sources contribute 73% of total inorganic NR-PM₁ (2.3 μg m⁻³) on
464 average during marine flow conditions.

465 Multiple lines of evidence support the use of MSA measurements coupled with the biogenic
466 MSA/nss-SO₄ ratio to apportion anthropogenic and biogenic nss-SO₄. Using measurements of
467 chlorophyll-*a* concentrations, wind speeds measured onboard the R.V. Brown, and the wind
468 speed/transfer velocity relationship determined by Nightingale et al. (2000), Bates et al. (2008)
469 estimated that the DMS flux from the Gulf of Mexico was capable of producing between 0.2 and
470 0.4 μg m⁻³ of biogenic nss-SO₄. For comparison, the average mass loading of biogenic nss-SO₄
471 calculated using the biogenic MSA/nss-SO₄ ratio during marine periods in our study is 0.54 μg

472 m^{-3} , in relatively good agreement with those results. Furthermore, Figure 5 shows the WPSCF
473 analysis of anthropogenic nss-SO₄ and MSA, the Automated Mutual Assistance Vessel Rescue
474 System (AMVER) shipping spatial proxy map (Wang et al., 2008), and chlorophyll-*a* levels
475 derived from MODIS satellite measurements. The use of the biogenic MSA/nss-SO₄ ratio is
476 qualitatively supported by the relatively distinct WPSCF results of anthropogenic nss-SO₄ and
477 MSA and by the agreement between the anthropogenic nss-SO₄ WPSCF map and the region of
478 high shipping traffic indicated by the AMVER inventory. The high probability region of
479 anthropogenic nss-SO₄ is located predominately outside of the ECA boundary where shipping
480 lanes converge, while the MSA high probability region is largely within the ECA where surface
481 chlorophyll-*a* concentrations are elevated (Figure 5).

482 While point-source emissions in Florida or long-range transport could contribute to the
483 anthropogenic nss-SO₄ measured during this study, further analysis suggests these sources are
484 minor in comparison to marine vessel emissions. According to the National Emissions Inventory
485 (NEI), ~160,000 tons of SO₂ were emitted in Florida in 2014 (U.S. EPA, 2014). However, only
486 ~30,000 tons (~19%) were emitted in the southern peninsular region indicated as a potential
487 source by the WPSCF analysis (south of 28°N) (Figure S17). While point-source distributed NEI
488 data are not yet available for 2016, EPA statewide average data suggest that Florida SO₂
489 emissions were approximately half of those in 2014 (~80,000 tons), with the change almost
490 entirely due to a 75% reduction in emissions from electricity generating stations (U.S. EPA,
491 2017). If emissions from individual electricity generating stations south of 28°N have been
492 similarly reduced, only ~20,000 tons of SO₂ were emitted in the southern peninsular region in
493 2016. For comparison, recent emissions inventories predict that marine vessels emit as much as

494 75,000 tons of SO₂ annually in the Gulf of Mexico after accounting for the ECA, nearly four
495 times as much as the geographically relevant Florida emissions (Johansson et al., 2017).

496 Offshore oil and gas extraction operations represent another source of SO₂ emissions
497 within the Gulf of Mexico. As can be seen from Figure 5, all currently operating offshore sites
498 are located within the NA-ECA (Wilson et al., 2017). Under the Clean Air Act, regulation of
499 currently operating offshore oil and gas sites is handled by the Department of the Interior's
500 Bureau of Ocean Energy Management (BOEM). According to the BOEM 2014 Gulfwide
501 Emission Inventory Study, annual SO₂ emissions from platform and non-platform oil and gas
502 operations totaled 7,150 tons (Wilson et al., 2017). Within the same study region, SO₂ emissions
503 from commercial marine vessels were estimated at 48,215 tons (Wilson et al., 2017). The
504 discrepancy between marine vessel SO₂ emissions reported in the BOEM inventory (48,215
505 tons) and that of Johansson et al. (2017) (75,000 tons) is due to the limited spatial scope of the
506 BOEM study (only the Western Gulf of Mexico was considered). While non-negligible, offshore
507 operations therefore represent less than ~15% of SO₂ emissions in the western Gulf of Mexico
508 and less than ~10% of total SO₂ emissions in the entire Gulf of Mexico.

509 In terms of the contribution from long-range transport, air masses that originated in Europe
510 or Africa required 15 days of transit or more to reach the measurement site based on HYSPLIT
511 modeling. Assuming that sulfur compounds have a lifetime of ~5-7 days in the MBL (Faloona,
512 2009), 89-95% of the original sulfur in these air masses would be lost prior to measurement. This
513 agrees with the finding by Bates et al. (2008) that only a small fraction of SO₄ measured in the
514 Gulf of Mexico was contributed by African dust during measurements in 2006.

515 Volcanic sources of SO₂ have occasionally contributed significantly to nss-SO₄ in marine
516 regions during previous campaigns (Jung et al., 2014). Any nss-SO₄ produced by volcanic

517 emissions would be apportioned to anthropogenic sources due to the apportionment technique
518 used (i.e., volcanoes would not be expected to produce substantial MSA, leading to a depression
519 of the MSA/nss-SO₄ ratio). Therefore, the influence of volcanic emissions would incorrectly
520 increase the fraction of measured nss-SO₄ attributed to anthropogenic sources. However, the only
521 relevant volcanoes in the area are along the Caribbean islands, and backward trajectory analysis
522 reveals that the largest measured mass loadings of nss-SO₄ correspond to air masses that passed
523 far north of them. It therefore appears that the vast majority of measured anthropogenic nss-SO₄
524 was emitted by marine vessels rather than other sources.

525 These results contrast with those from the previous model study of Lauer et al. (2007), who
526 predicted using a global model that shipping contributes only ~30% of submicron SO₄ over the
527 Gulf of Mexico using the AMVER-distributed shipping inventory from Eyring et al. (2005) and
528 as little as 15% or less using the International Comprehensive Ocean-Atmospheric Dataset-
529 distributed inventory from Corbett and Kohler (2003) on an annual basis. Multiple lines of
530 evidence suggest that the discrepancies observed between our results and previous modeling
531 results are not simply due to the timing of our measurements. For instance, while less shipping-
532 related SO₄ is likely produced in the fall/winter due to the reduction in photochemical activity
533 during that time, conversion of biologically-emitted SO₂ into nss-SO₄ should have the same
534 photochemical dependence. Furthermore, the SO₂ yield from DMS oxidation, the major
535 biological nss-SO₄ production pathway, is reduced in the winter due to the temperature
536 dependence of DMS oxidation chemistry, as previously explained (Section 2.8) (Jung et al.,
537 2014). Finally, data from the Port of Houston suggests that shipping traffic (estimated by the
538 number of twenty-foot equivalent cargo units (TEUs) processed at the port) is only reduced by
539 ~10% in the winter (Figure S18) (Port of Houston, 2017). However, a portion of this discrepancy

540 is likely attributable to the fact that the marine period of our study only encompasses onshore
541 flow conditions, whereas the annual average calculated by Lauer et al. (2007) also incorporates
542 periods of offshore flow, when continental emissions act as source of nss-SO₄ to the MBL over
543 the Gulf of Mexico.

544 Quantification of anthropogenic nss-SO₄ allows for a more detailed apportionment of marine
545 OA than was possible based on MSA alone. While the correlation between total nss-SO₄ and
546 OOA-3 (the dominant marine OA factor) is moderate ($R^2 = 0.55$), anthropogenic nss-SO₄ is
547 strongly correlated with OOA-3 ($R^2 \geq 0.78$) (Figure S12), suggesting OOA-3 is coupled to
548 shipping emissions either directly (e.g., SOA from marine vessel VOCs or oxidation of
549 evaporated marine POA) or indirectly (e.g., increased uptake of water soluble gases over the
550 MBL due to increased ALW). Substantial processing of OOA-3 during transport leads to the
551 removal of major mass spectral tracers; however, there is some evidence for a contribution from
552 naphthalene OA (discussed in the SI), which is a dominant commonly-measured VOC emitted
553 by major commercial shipping vessels (Agrawal et al., 2008; Murphy et al., 2009; Czech et al.,
554 2017). Assuming, as a strictly upper bound estimate, that OOA-3 production is entirely
555 dependent on shipping emissions, anthropogenic sources contributed 71% of total NR-PM₁ (2.7
556 $\mu\text{g m}^{-3}$) on average during the marine period.

557 Comparing the submicron mass loadings of nss-SO₄ and NH₄ measured during marine
558 periods by Bates et al. (2008) (pre-ECA) ($3 \mu\text{g m}^{-3}$) to those measured during our study ($3.04 \mu\text{g}$
559 m^{-3}) suggests ECA implementation has had a negligible effect on aerosol mass. However, the
560 amount of shipping traffic within the Gulf of Mexico, estimated with the total number of loaded
561 TEUs processed at the ports of Houston, TX, Galveston, TX, Freeport, TX, New Orleans, LA,
562 and Mobile, AL has increased by approximately 42% since 2006 (Figure S19) (U.S. Army Corps

563 of Engineers, Navigation Data Center, 2016), suggesting that emissions reductions per vessel
564 within the ECA boundary may have been offset by increased traffic. On a yearly basis, the
565 estimated increase in shipping traffic since 2006 (4.6% per year) is similar to the annual growth
566 in seaborne trade observed between 2002 and 2007 (5.2%) and is within the range of growth
567 predicted through 2050 (3.6-5.9%) (Corbett et al., 2007; Eyring et al., 2010). In support of these
568 rapid growth estimates, Tournadre (2014) recently concluded that shipping traffic in the Atlantic
569 Ocean nearly doubled between 2006 and 2012, corresponding to an average annual increase of
570 ~8%. While it is also possible that the specific meteorological conditions encountered during this
571 campaign (i.e., air mass trajectories, average wind speeds, etc.) were more conducive to the
572 accumulation of anthropogenic nss-SO₄ than during the study of Bates et al. (2008), this is
573 unlikely to be the dominant reason for the little change observed since ECA implementation.
574 Therefore, our results suggest that the ECA has reduced shipping emissions on a per vessel basis,
575 as there has been little change in shipping-related aerosol despite significant growth in the
576 shipping trade. These results also provide justification for further limits on FSC, which are
577 expected to be implemented in 2020 and require a reduction of FSC to a maximum of 0.5%
578 globally (Kotchenruther, 2016). However, longer term observational or modeling studies are
579 nevertheless needed to more definitively quantify the effect of the ECA.

580 **3.4 Relationship Between Shipping Emissions and OA Oxidation State**

581 In order to obtain a quantitative measure of the difference in OA composition between air
582 masses influenced by shipping emissions and those lacking such influence, a 12-hour period was
583 isolated on 6/10-6/11 when the site encountered air masses that had been inside the ECA
584 boundary but over the ocean (i.e., within 200 nautical miles of the coast) for virtually their entire
585 five-day history (Figure S20). Assuming ECA compliance, these air masses should receive only

586 a small fraction of the particulate and SO₂ emissions encountered by those originating outside the
587 boundary (Lack et al., 2009; Lack et al., 2011; Browning et al., 2012). Based on air mass history
588 and the accompanying mass spectral analysis described below, we classified OA measured
589 during this period as “marine-biogenic.” For comparison, we distinguished a second 24-hour
590 period (5/30) that had similar 5-day backward-trajectory-averaged meteorological conditions to
591 the biogenic period (faster average wind speed and comparable average solar flux) but had
592 trajectories that originated outside the ECA boundary and passed through the high intensity
593 shipping region. The shipping-influenced period had notably larger mass loadings of
594 anthropogenic nss-SO₄ (2.24 versus 1.09 μg m⁻³) and OA (1.04 versus 0.29 μg m⁻³).

595 Figure 6 presents the average OA mass spectra determined for each of these periods. In the
596 shipping-influenced air masses, measured OA is highly processed, with a much larger f₄₄ (0.20)
597 (a marker of carboxylic acids) than is typical of marine biogenic OA (~0.08-0.14) (Chang et al.,
598 2011; Coggon et al., 2012; Crippa et al., 2013; Coggon et al., 2014) and a composition
599 dominated by oxygenated species (66%). In contrast, OA measured during the period of minor
600 shipping influence is notably less aged and contains numerous indicators of a marine biogenic
601 source. For instance, prominent non-oxygenated spectral fragments are observed at m/z 27, 39,
602 41, 43, 55, and 67 (Figure S21) implying the presence of alkenes, cycloalkenes, cycloalkanes,
603 and dienes, in agreement with Ovadnevaite et al. (2011, 2014) for marine OA measured at Mace
604 Head, Ireland and by Bates et al. (2012) in physically generated sea spray aerosol. A relatively
605 significant contribution from m/z 79 (CH₃SO₂) (~1%) is also apparent, and as a result MSA
606 contributes 9.3% of total OA, a value three times larger than the average during the marine
607 period, and in closer agreement with previous measurements in remote marine regions
608 (Ovadnevaite et al., 2014). Furthermore, a prominent signal from the CHO⁺ ion, an aldehyde

609 tracer, is observed (~7%), which is uncharacteristic of aged urban emissions (Ng et al., 2010) but
610 has been observed in the mass spectra of numerous biogenic SOAs from both chamber
611 experiments and ambient measurements (Shilling et al., 2009; Chhabra et al., 2010; Slowik et al.,
612 2010; Setyan et al., 2012) and from marine biogenic OA specifically (Chang et al., 2011; Crippa
613 et al., 2013; Coggon et al., 2014). Ultimately, the biogenic period spectra correlates well with the
614 marine biogenic factor extracted by Chang et al. (2011) over the Arctic Ocean ($R^2 = 0.78$) as
615 well as with the marine OA factor extracted by Crippa et al. (2013) in Paris ($R^2 = 0.68$), while
616 the shipping-influenced period spectra correlates extremely well with the continental factor
617 extracted by Chang et al. (2011) ($R^2 = 0.95$).

618 The mass spectra from the shipping-influenced period has notably larger signals from m/z 44
619 and m/z 28 than the biogenic period, suggesting a larger amount of atmospheric processing that
620 converted OA components into organic acids (Chhabra et al., 2011). Numerous remote marine
621 studies have shown that on average, the oxidation state of marine aerosol varies only slightly in
622 the absence of anthropogenic influences (Gantt and Meskhidze, 2013; Wozniak et al., 2014). In
623 this case, the absolute difference in the O:C ratio between the two scenarios is 0.29 (0.90 for the
624 shipping-influenced period versus 0.61 for marine-biogenic), implying a major impact of
625 shipping on related OA chemical and potentially physical properties. While primary marine
626 aerosol particles can have high O:C ratios (~1) due to the significant mass fraction of
627 carbohydrate components in dissolved organic matter (Russell et al., 2010), the low trajectory-
628 averaged wind speeds and high f_{44} suggest that OA measured during the shipping-influenced
629 period is not primary (Frossard et al., 2014).

630 Using the function developed by Duplissy et al. (2011) to describe the relationship between
631 OA oxidation state (represented by the mass fraction of m/z 44) and hygroscopicity, the

632 calculated hygroscopic growth factor (κ_{org}) for the shipping-influenced period is three times
633 larger (0.31 versus 0.101) than that calculated for the marine-biogenic period. Therefore, despite
634 the fact that freshly emitted in-plume shipping aerosol is thought to have a suppressed
635 hygroscopic growth factor relative to background marine aerosol (Murphy et al., 2009), our
636 results suggest that extensive aging during transport near shipping lanes (presumably due to
637 increased oxidant levels) may lead to an eventual increase in bulk marine OA hygroscopicity
638 relative to aerosol unaffected by shipping emissions. This hypothesis is supported by the
639 relatively strong correlation observed between daily anthropogenic nss-SO₄ and the organic
640 hygroscopicity factor ($R^2 = 0.64$) calculated using the Duplissy et al. (2011) method during the
641 marine period (Figure 7).

642 Figure 8 displays marine OA plotted on the f_{44} versus f_{43} triangle diagram (Ng et al., 2010) to
643 describe OA aging. Less oxidized OA typically occupies a wide space at the bottom of the plot,
644 indicative of variable ambient OA mass spectra, while aging causes movement diagonally
645 upward, as mass spectra become more similar with age (Ng et al., 2010). Figure 8 highlights that
646 OA oxidation is greatly influenced by a combination of physical air mass history and
647 meteorology. Three specific days demonstrate these influences particularly well. On 5/24,
648 backward trajectory analysis reveals that air masses passed directly over the region of major
649 shipping influence, resulting in a substantial amount of nss-SO₄ aerosol and highly oxidized OA.
650 In contrast, on 6/11, despite the fact that trajectory-averaged wind speeds were lower and solar
651 flux was comparable, suggesting meteorological conditions were more conducive to OA
652 processing and elevated aerosol mass loadings, air masses largely missed the high intensity
653 shipping region (and remained largely within the ECA), resulting in less nss-SO₄ and less-
654 oxidized OA. On 6/13, arriving air masses had faster average wind speeds and avoided shipping

655 lanes, resulting in an extreme case of very little nss-SO₄ and only minor processing. Based on
656 this information, it appears that air mass transit within major shipping corridors is associated
657 with more processed organic aerosol relative to background marine conditions in the Gulf of
658 Mexico.

659 There are multiple ways in which the presence of shipping emissions could increase the rate
660 of OA processing. While peak daytime concentrations of OH of 6×10^6 - 1×10^7 mol cm⁻³ are
661 relatively consistent throughout the clean MBL (Raper et al., 2001; Vaughan et al., 2012),
662 modeling results by Chen et al. (2005) and Kim et al. (2013) indicate that within individual
663 shipping plumes, OH concentrations are elevated by a factor of 1.2 to 2.7, and OH
664 concentrations can remain elevated up to 140 km behind an individual shipping vessel.
665 Significant NO₂ levels within the plume also increase concentrations of nitrate radical to several
666 pptv, even during the daytime, which would hypothetically result in rapid oxidation of any
667 unsaturated VOCs or components of primary marine OA (Myriokefalitakis et al., 2010; Bates et
668 al., 2012; Kim et al., 2013). Additionally, elevated production of nss-SO₄ aerosol increases
669 ambient ALW mass, increasing the partitioning medium available to small, water-soluble
670 organic gases (WSOG) produced from both biogenic and anthropogenic sources (i.e., glyoxal,
671 methylglyoxal, acetaldehyde, etc.) and processed in the aqueous phase into highly oxidized
672 species (such as glyoxylic acid/glyoxylate, O:C = 1.5, or oxalic acid/oxalate, O:C = 2) (Ervens et
673 al., 2011; Ge et al., 2012).

674 However, it should be noted that unlike SO₂ emissions/concentrations, the presence of the
675 ECA may not substantially reduce concentrations of atmospheric oxidants within shipping
676 plumes. Numerous studies have linked shipping-related perturbations of marine OH radical
677 concentrations to vessel NO_x emissions (e.g., Lawrence and Crutzen, 1999; Kim et al., 2013).

678 While Tier III NO_x emissions standards implemented in the ECA in 2016 are projected to slowly
679 reduce emissions over time (as standards only apply to vessels constructed in 2016 and later),
680 Browning et al. (2012) have shown that the sole switching from high sulfur HFO to MGO at the
681 ECA border in the Gulf of Mexico only produced NO_x reductions of 1-6%. As a result, the effect
682 of shipping emissions on marine OA processing likely depends more on whether air masses align
683 with shipping lanes during transit than whether such transit occurs within or outside of the
684 current ECA.

685 **3.5 Relationship Between Shipping Emissions and Major Marine OA Components:**

686 **Amines and MSA**

687 While MSA and alkyl-amines, such as dimethyl-amine (DMA) and diethyl-amine
688 specifically, are frequently observed over the MBL and are linked to biogenic emissions
689 (Murphy et al., 2007; Facchini et al., 2008; Sorooshian et al., 2009), the partitioning dynamics of
690 each are influenced by shipping emissions. For instance, recent single particle measurements in
691 California reveal a possible catalytic role of vanadium in MSA formation (Gaston et al., 2010),
692 while gaseous alkyl-amines typically undergo neutralization reactions with sulfuric or nitric
693 acids to form aminium salts (Murphy et al., 2007). However, previous studies have produced
694 conflicting results about whether biogenic marine SOA mass is maximized in clean or polluted
695 environments. For instance, Sorooshian et al. (2009) and Facchini et al. (2008) both noted that
696 mass loadings of amines and MSA were largest in clean rather than polluted air masses,
697 supporting their attribution to biogenic sources; however, Sorooshian et al. (2015a) observed
698 similar size distributions of MSA and vanadium along the California coast, while Youn et al.
699 (2015) reported noticeable long-term correlations between amines and SO₄. Myriokefalitakis et
700 al. (2010) suggested that on a global basis, modeled marine SOA originates almost entirely from

701 either DMS oxidation (i.e., MSA-related) (~78%) or formation of dialkyl amine salts (~21%),
702 highlighting the importance of understanding anthropogenic influences on their production in
703 areas influenced heavily by ship traffic. To quantify a lower-bound ambient amine signal from
704 this coastal dataset, individual mass spectral fragments typical of alkyl amines identified in
705 previous HR-ToF-AMS studies, specifically those at m/z 27 (CHN^+), 30 (CH_4N^+), 44 ($\text{C}_2\text{H}_6\text{N}^+$),
706 56 ($\text{C}_3\text{H}_6\text{N}^+$), 58 ($\text{C}_3\text{H}_8\text{N}^+$), and 72 (CH_4N_4^+), were combined (Murphy et al. 2007; Hildebrandt
707 et al., 2011; Sun et al., 2011).

708 Figure 9 highlights that hourly-averaged amine mass loadings correlate well with
709 anthropogenic nss-SO_4 ($R^2 = 0.63$) while MSA mass loadings show a noticeably weaker
710 relationship ($R^2 = 0.30$). A strong correlation between MSA and anthropogenic nss-SO_4 would
711 indicate that either the biogenic nss-SO_4 fraction had been under-predicted or that a strong
712 catalytic effect on MSA production was occurring.

713 The correlation between anthropogenic nss-SO_4 and amines is consistent with those observed
714 by Youn et al. (2015) for DMA and SO_4 in Tucson, AZ, in 2013 ($r \geq 0.72$). Amines also display
715 a positive relationship with NH_4 ($R^2 = 0.61$, similarly to nss-SO_4), in agreement with the fact that
716 throughout the campaign, NR-PM_{10} was never fully neutralized by the small ammonia sources
717 that exist over the MBL. This is highlighted by the fact that the average neutralization ratio, the
718 molar ratio of ammonium to the sum of sulfate and nitrate ($[\text{NH}_4^+]/(2 \times [\text{SO}_4^{2-}] + [\text{NO}_3^-])$), was
719 only 0.74, resulting in a consistent pathway for amine SOA formation through aqueous
720 dissolution and partial neutralization of the acidic nss-SO_4 aerosol. Furthermore, the correlation
721 between amines and anthropogenic nss-SO_4 is much stronger than correlations with average
722 wind speed, solar flux, and mixing layer depth ($R^2 = 0.04, 0.18, \text{ and } 0.10$ respectively),

723 suggesting that anthropogenic emissions play a larger role in amine aerosol formation than
724 meteorology.

725 The link between shipping emissions and amine formation also is supported by the high
726 nitrogen to carbon ratio (N:C) of the dominant marine PMF factor, OOA-3 (N:C = 0.074), a
727 value larger than that observed in aged marine OA (N:C ~0.04) (Schmale et al., 2013) and
728 amine-related urban PMF factors extracted in Pasadena, CA (N:C = 0.052) (Hayes et al., 2013)
729 and New York City (N:C = 0.053) (Sun et al., 2011), but similar to a biogenic MSA-related
730 factor extracted at Bird Island near Antarctica (N:C = 0.08) (Schmale et al., 2013). It is likely
731 that this anthropogenic-biogenic link can be extrapolated to other areas where marine biogenic
732 and shipping emissions coexist. As a result, amines measured in heavily trafficked marine
733 environments should not be interpreted exclusively as products of a purely biogenic SOA
734 formation pathway.

735 **3.6 Anthropogenic ALW and Potential Influences on SOA formation**

736 While the impacts of shipping emissions on marine cloud condensation nuclei
737 concentrations, cloud formation processes (e.g., ship tracks) and cloud properties (e.g., increased
738 albedo, increased droplet acidity) have been extensively studied in the recent past (e.g., Coakley
739 et al., 1987; Durkee et al., 2000; Coggon et al., 2012; Peters et al., 2012; Sorooshian et al.,
740 2015b), there have been few measurement-based analyses of the role of these emissions on the
741 production of ALW and subsequent OA processing in coastal marine environments. The
742 injection of SO₂ and production of SO₄ aerosol mass in the marine boundary layer, combined
743 with high ambient relative humidity levels, will lead to a substantial mass concentration of ALW
744 associated with submicron anthropogenic particles, even in cloud-free conditions. As organic
745 gases capable of partitioning to ALW are present throughout the MBL (Sinreich et al., 2010),

746 have elevated concentrations near the coasts (Fu et al., 2008; Fu et al., 2011), and contribute
747 significantly to aerosol mass in both rural and urban areas within the southeastern United States
748 (Li et al., 2015), the production of this partitioning medium over the marine boundary layer may
749 impact SOA production. As a result, measurement-based modeling of ALW is needed to inform
750 understanding of how future changes to shipping sulfur emissions might influence SOA
751 formation in coastal environments.

752 On average, ALW mass loadings of $5.21 \pm 4.62 \mu\text{g m}^{-3}$ are modeled using ISORROPIA II
753 (Fountoukis and Nenes, 2007) during the marine period, representing on average 58% of total
754 NR-PM₁ particle mass. This value is slightly larger than the average determined for the HSC
755 region in September-October 2006 by Nguyen et al. (2016) ($4.6 \mu\text{g m}^{-3}$), presumably because of
756 higher average RH along the coast and similar total inorganic mass loadings, and is larger than
757 the average values reported for every major city in North America analyzed by Nguyen et al.
758 (2016). If anthropogenic nss-SO₄ were eliminated completely, average ALW mass loadings
759 associated with NR-PM₁ aerosol would ultimately be reduced by 66.4%. As a result, the majority
760 of NR-PM₁-associated ALW over the Gulf of Mexico appears to be controllable. While
761 concentrations of WSOG over the MBL are relatively small (Sinreich et al., 2010), advection of
762 this ALW inland may have large impacts on nearby SOA formation where precursor sources are
763 more prevalent.

764 Multiple modeling studies have suggested that small WSOG, specifically glyoxal,
765 methylglyoxal, and isoprene epoxides (IEPOX), contribute heavily to SOA mass in the Houston
766 region (Li et al., 2015; Ying et al., 2015). Li et al. (2015) found that these three compounds were
767 responsible for nearly 80% of total SOA mass loadings at a downtown site during a simulated
768 period in 2006, with the largest fraction (~30-50%) contributed by IEPOX. The authors also

769 showed that these species dominate SOA mass across the Gulf Coast, with significant total
770 loadings ($\sim 4 \mu\text{g m}^{-3}$ or greater) from the southern end of Texas to the Florida panhandle. Ying et
771 al. (2015) used the Community Multi-scale Air Quality model (CMAQ) to characterize biogenic
772 and anthropogenic contributions to glyoxal and methylglyoxal SOA and found that isoprene is a
773 major contributor to both (47% of glyoxal and 82% of methylglyoxal SOA, specifically). As
774 these compounds are precursors to aqueous SOA (aqSOA) formation, anthropogenic impacts on
775 ALW represent another potential anthropogenic-biogenic link in SOA production (Carlton and
776 Turpin, 2013).

777 The aqSOA formation from these WSOG ultimately depends on both uptake into ALW
778 and subsequent reactions to produce low-volatility organic acids or high-molecular weight
779 oligomeric products (McNeill, 2015). However, as uptake of OH, the dominant aqueous phase
780 oxidant, is typically surface-limited (Ervens et al., 2014), large scale models often simplify this
781 process by assuming that aqSOA formation is irreversible and surface-controlled (Li et al., 2015;
782 Ying et al., 2015), representing SOA production rate by

$$783 \quad \frac{dM_{a,i}}{dt} = \frac{1}{4} \gamma_i v_i A M_i \quad (4)$$

784 where $M_{a,i}$ is the aerosol-phase mass concentration of species i ($\mu\text{g m}^{-3}$), γ_i is its reactive uptake
785 coefficient, v_i is its gas-phase thermal velocity (m s^{-1}), A is the ambient aerosol surface area
786 concentration ($\text{m}^2 \text{m}^{-3}$), and M_i is the mass concentration of the species in the gas phase ($\mu\text{g m}^{-3}$).
787 As a fraction of WSOG partitioning is reversible (Chhabra et al., 2010; Wong et al., 2015), and
788 SOA formation may be more dependent on the particle-phase reaction rate than simply the
789 particle surface area (SA) (Budisulistiorini et al., 2017), this estimated production rate likely
790 represents an upper limit; however, published CMAQ results for OA mass loadings in the

791 Houston area calculated in this manner agree well with observations (Li et al., 2015; Ying et al.,
792 2015).

793 In order to approximate the effect of anthropogenic marine aerosol (AMA) on WSOG
794 aqSOA production, we modeled aqSOA formation from isoprene-derived glyoxal,
795 methylglyoxal, and IEPOX in the Houston area using the equation above and a previously
796 developed 0-D model including a semi-explicit isoprene oxidation mechanism (Schulze et al.,
797 2017). This model assumes that air masses rich in AMA advect over the urban core of Houston,
798 where the added SA due to anthropogenic emissions over the ocean increases SA-dependent
799 aqSOA production rates. Total model SA was quantified by combining the dry mass size
800 distribution measured by the HR-ToF-AMS at the coastal site during onshore flow and the mass
801 added by NR-PM₁-associated ALW; however, a correction was applied to account for SA loss
802 due to deposition and ALW evaporation during transport to the HSC. A detailed description of
803 all model assumptions (i.e., boundary layer height, aerosol deposition and ALW evaporation
804 during transport, etc.) is provided in the SI. Average diurnal isoprene, O₃, and NO_x
805 concentrations measured by five monitors within the HSC during the marine period were used as
806 model constraints (Figure S22). Diurnal OH concentrations were taken from measurements in
807 downtown Houston during the SHARP 2009 campaign (Ren et al., 2013).

808 A diurnal model run was first performed using the total corrected marine aerosol SA to
809 predict aqSOA formation in the HSC. This procedure isolates aqSOA production due to marine
810 aerosol SA specifically. In order to produce an upper bound estimate of the effect of AMA, a
811 second run was performed with all SA contributions from anthropogenic species removed (i.e.,
812 anthropogenic nss-SO₄, NH₄, and ALW), and the difference in aqSOA was calculated. A lower
813 bound estimate was calculated with a model run that only removed the SA contribution of

814 anthropogenic ALW. In order to ensure conservative results, OA was assumed to be entirely
815 biogenic for the purposes of this calculation.

816 To compare this effect with SOA production from locally-emitted anthropogenic VOCs
817 (AVOC-SOA) in Houston, gas-phase AVOC data measured during the marine period
818 (concentrations of 16 alkanes, 7 alkenes, and 9 aromatics) was obtained from the same
819 monitoring sites around the HSC (Figure S22). Estimates of SOA production rates from these 32
820 VOCs were calculated using the volatility basis set approach utilized in Tsimpidi et al. (2010). In
821 this mechanism, organic condensable gases produced from initial VOC oxidation are allowed to
822 undergo further aging to produce lower volatility products (Tsimpidi et al., 2010; Hayes et al.,
823 2015). A more detailed description of this process is provided in the SI.

824 Figure 10 shows that on a daily basis, aqSOA production attributable to isoprene WSOG
825 reactive uptake is primarily due to methylglyoxal rather than IEPOX, implying “high-NO_x”
826 rather than “low-NO_x” ambient conditions (Budisulistiorini et al., 2017). Assuming high-NO_x
827 conditions, the modeled effect of AMA on aqSOA production in the HSC is equivalent to 6-23%
828 of potential daily SOA production from AVOCs measured locally. Using data from the monitor
829 with the highest isoprene concentrations (Haden Road; Figure S24), we predict that the AMA
830 effect may constitute as much as 11-43% of total AVOC-SOA production, implying strong
831 spatial variability in the relative contribution of this effect. Modeled AVOC-SOA production
832 peaks in the early afternoon, consistent with the fact that the aging of condensable gases formed
833 by measured VOCs produces the majority (~80%) of modeled AVOC-SOA.

834 Recent studies have revealed that a substantial fraction of SOA formation in urban
835 environments may be produced by primary anthropogenic semi-volatile/intermediate volatility
836 VOCs (P-S/IVOCs) co-emitted with typical VOCs or evaporated during POA dilution but not

837 typically measured (Hayes et al., 2015 and references therein). In Los Angeles, for instance,
838 Hayes et al. (2015) predicted that P-S/IVOCs comprise between 44% and 92% of total modeled
839 SOA depending on the specific SOA formation mechanism used. As a result, the relative
840 magnitude of the AMA effect may be somewhat overestimated here. Still, the AMA effect is
841 responsible for 0.2-0.35 $\mu\text{g m}^{-3}$ of ambient aqSOA according to the model calculations, which
842 represents 4-6% of ambient OA measured by Cleveland et al. (2012) near downtown, ~3-5% of
843 OA modeled using CMAQ by Li et al. (2015), and as high as ~10-17% of average OA measured
844 in Houston's urban core by Leong et al. (2017). Furthermore, as AVOCs such as benzene and
845 acetylene are known to produce glyoxal and methylglyoxal with high yields (Fu et al., 2008), the
846 total OA mass attributable to AMA through this pathway (on an absolute rather than relative
847 basis) may actually be larger than predicted here. Our results therefore suggest that future
848 reductions in marine nss-SO₄ may reduce aqSOA formation in both urban (e.g., Houston) and
849 forested regions across the Gulf Coast.

850

851 **4 Conclusions**

852 Three weeks of continuous measurements with an HR-ToF-AMS at a coastal location
853 near Houston, TX were used to gain further insight into the impact of shipping emissions on
854 coastal aerosol properties. Measured mass loadings of inorganic NR-PM₁ components were
855 similar to those reported before establishment of the ECA within the Gulf of Mexico; however,
856 data from nearby ports suggests that this is the result of growth in the shipping trade rather than
857 regulatory ineffectiveness on a per vessel basis. Using MSA calibrations and published biogenic
858 MSA/nss-SO₄ ratios, we predict that over 70% of inorganic marine NR-PM₁ is anthropogenic
859 rather than biogenic. Source apportionment using PMF revealed that the dominant marine OA

860 factor (OOA-3) is highly correlated with calculated anthropogenic nss-SO₄ ($R^2 \geq 0.78$),
861 supporting a link between shipping emissions and SOA production. Assuming, as an upper
862 bound estimate, that OOA-3 production is entirely dependent on shipping emissions,
863 anthropogenic sources contribute over 70% of total measured NR-PM₁ during onshore flow,
864 despite the regulations. This suggests that the proposed future global decrease in shipping FSC
865 (decrease to 0.5%) should substantially reduce PM levels over the Gulf of Mexico. However,
866 longer term studies are warranted to fully investigate this possibility.

867 Shipping emissions were also found to have numerous secondary effects on OA
868 composition. Detailed backward trajectory and mass spectral analysis revealed that air mass
869 transit within shipping lanes leads to more processed (i.e., oxidized) OA than is encountered in
870 “clean” marine air masses, and calculations suggest that this aging increases OA hygroscopicity.
871 In addition, marine alkyl amine aerosol formation in the Gulf of Mexico appears to depend on
872 ambient anthropogenic nss-SO₄ mass, implying that marine amine aerosol cannot be viewed as
873 purely biogenic in heavily trafficked marine environments. OOA-3 was found to have a larger
874 N:C ratio than is typical of aged marine components, supporting this link. Finally, modeling
875 suggests that inland advection of shipping-related nss-SO₄ and related ALW may enhance
876 aqSOA formation and produce 4 to 17% of OA in the urban core of Houston during marine flow
877 for the conditions considered. Future detailed three-dimensional modeling studies are
878 recommended to better quantify this effect.

879

880

881 Acknowledgements:

882

883 The authors would like to acknowledge J. Stutz and K. Tuite (UCLA) for
884 assistance and helpful discussions during the field campaign. This material is based upon work
885 supported by the National Science Foundation Graduate Research Fellowship under Grant No.
886 DGE# 1450681.

887
888
889
890
891
892
893
894
895
896
897
898
899
900
901
902
903
904
905
906
907
908
909
910
911
912
913
914

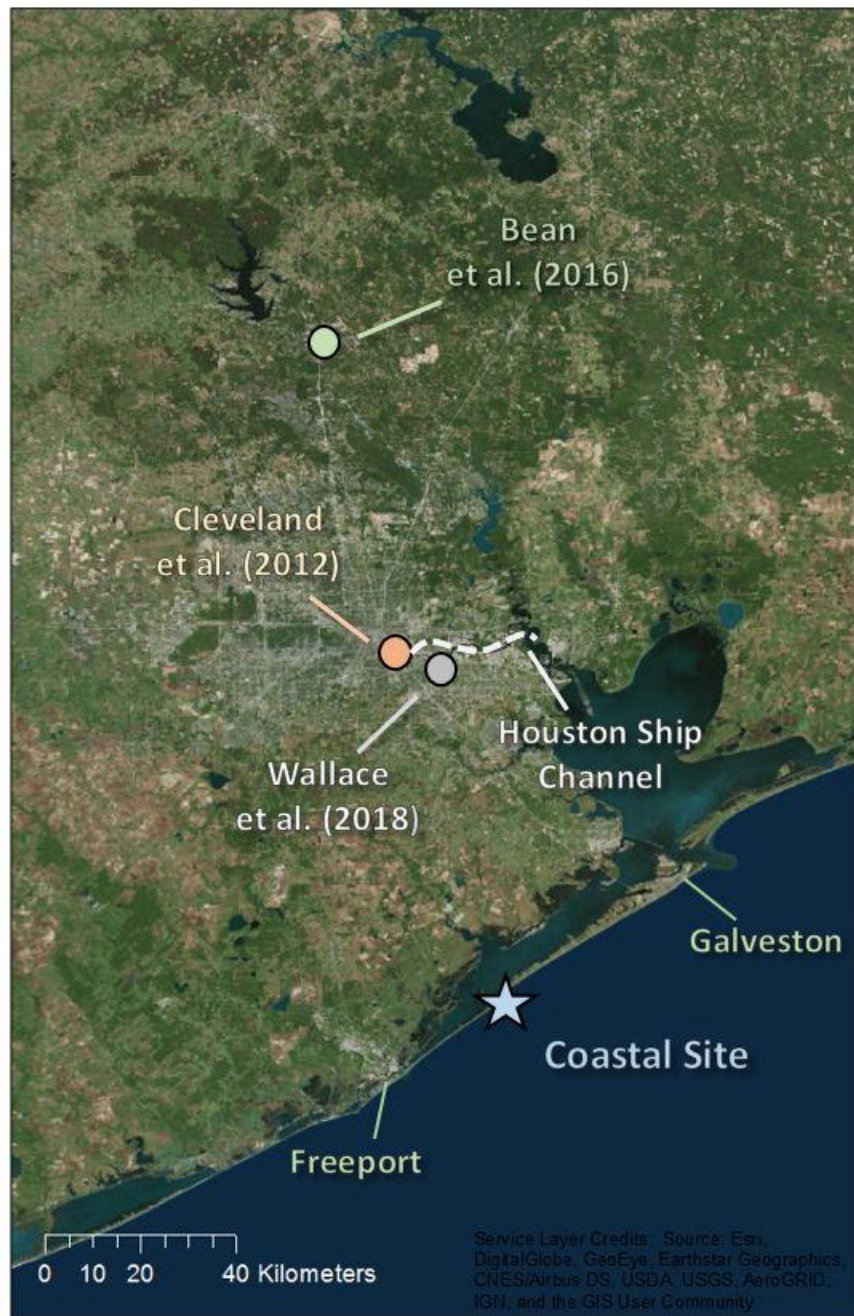


Figure 1: Map depicting the Houston region, the coastal study site (star), and the location of recent stationary campaigns that characterized aerosol dynamics in Houston.

915
916
917
918
919
920
921
922
923
924
925
926
927
928
929
930
931
932
933
934
935
936
937
938
939
940
941
942

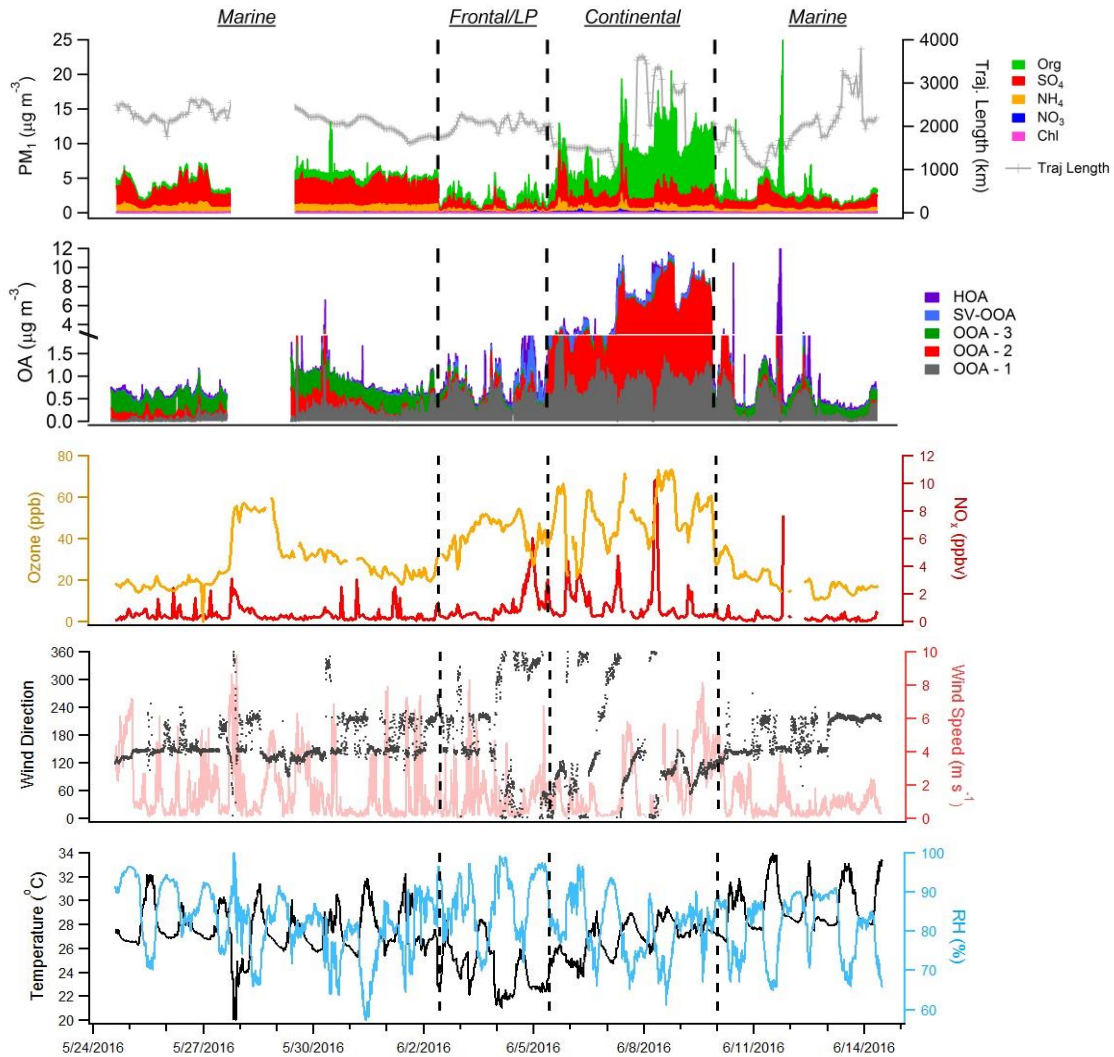


Figure 2: From top to bottom, time series of major NR-PM₁ species, extracted PMF factors, O₃ and NO₂, and meteorological variables (wind direction, wind speed, RH, and temperature) measured during the campaign. Dotted lines distinguish distinct time period types described in Section 3.1.

943
 944
 945
 946
 947
 948
 949
 950
 951
 952
 953
 954
 955
 956
 957
 958
 959
 960
 961
 962
 963
 964
 965
 966
 967
 968
 969
 970

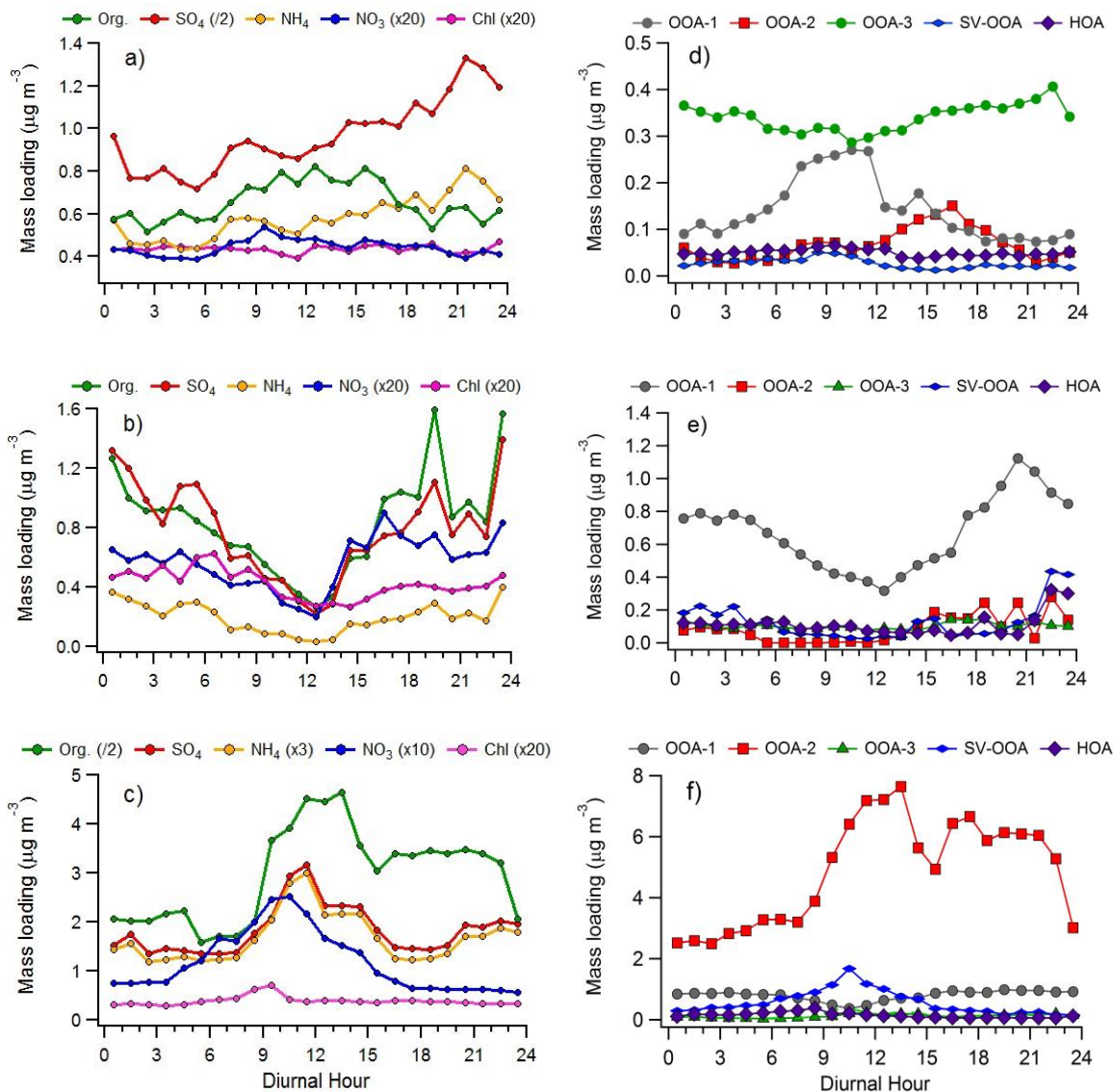


Figure 3: Diurnal variation of NR-PM₁ component average concentrations (a-c) and PMF factors (d-f) during the marine period (a & d), the frontal/LP period (b & e), and the continental period (c & f). The legends above a-c describe how mass loadings of specific components were adjusted to fit the figure. Note the different y-axis ranges applicable to each period type.

971

972

973 **Table 1:** Aerosol ($\mu\text{g m}^{-3}$) and trace gas (ppbv) characteristics (avg. \pm std. dev.) measured during
974 each distinct period type of the campaign.

Period	NR-PM ₁	OA	SO ₄	NH ₄	NO ₃	Chl.	O ₃	NO _x	CO
Marine	3.8 \pm 2.0	0.7 \pm 0.8	2.4 \pm 1.1	0.7 \pm 0.3	0.02 \pm 0.01	0.02 \pm 0.01	31.1 \pm 11.9	0.4 \pm 1.2	111.5 \pm 16.5
Frontal/LP	2.6 \pm 2.1	1.0 \pm 0.9	1.3 \pm 1.2	0.3 \pm 0.4	0.04 \pm 0.03	0.02 \pm 0.01	43.8 \pm 11.1	1.0 \pm 1.3	107.2 \pm 14.4
Continental	9.9 \pm 2.9	7.2 \pm 2.8	1.9 \pm 0.7	0.6 \pm 0.2	0.1 \pm 0.1	0.02 \pm 0.01	52.7 \pm 12.7	1.3 \pm 1.8	141.3 \pm 26.2

975

976

977

978

979

980

981

982

983

984

985

986

987

988

989

990

991

992

993

994

995

996

997

998 **Table 2:** Elemental composition of each PMF factor and contributions to total OA during each period
999 of the campaign

	Elemental Analysis			Marine Period		Frontal/LP Period		Continental Period	
	O:C	H:C	N:C	%	$\mu\text{g m}^{-3}$	%	$\mu\text{g m}^{-3}$	%	$\mu\text{g m}^{-3}$
OOA – 1	1.16	1.29	0.013	21	0.14	65	0.63	15	1.10
OOA – 2	0.79	1.41	0.007	11	0.08	6	0.06	72	5.21
OOA – 3	0.76	1.44	0.077	55	0.40	11	0.11	2	0.15
SV – OOA	0.43	1.77	0.013	3	0.02	9	0.09	8	0.60
HOA	0.08	1.89	0.002	7	0.05	9	0.09	2	0.16

1000

1001

1002

1003

1004

1005

1006

1007

1008

1009

1010

1011

1012

1013

1014

1015

1016

1017

1018

1019

1020

1021

1022

1023

1024

1025

1026

1027

1028

1029

1030

1031

1032

1033

1034

1035

1036

1037

1038

1039

1040

1041

1042

1043

1044

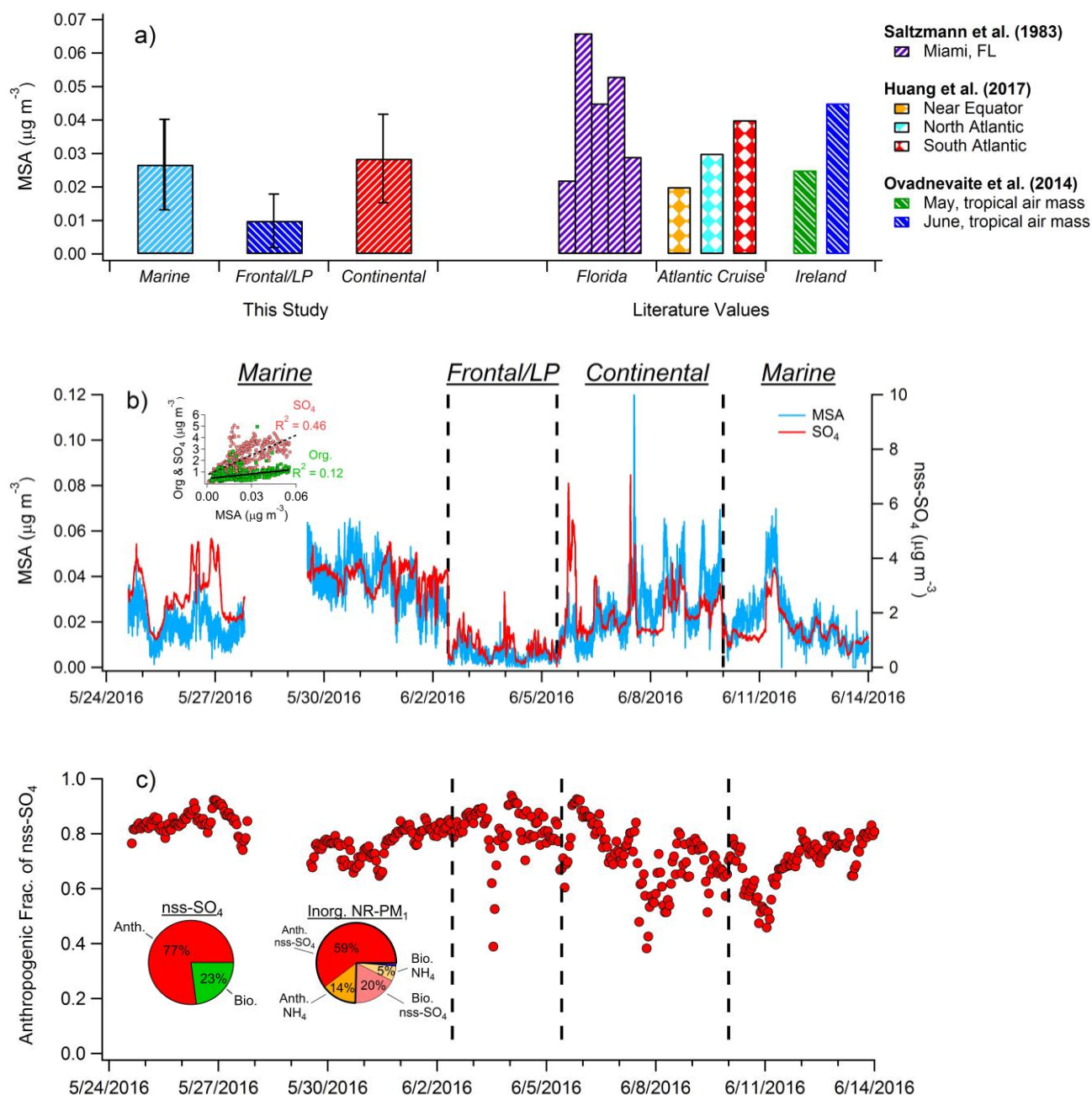


Figure 4: a) Comparison of average MSA mass loadings measured during each of the three major periods of the campaign with previously published values measured in Florida, on an Atlantic Cruise, and at Mace Head, Ireland. b) Time series of MSA and nss-SO₄. Black dashed lines denote boundaries of distinct time period types. Inset graph shows the correlation of total OA and SO₄ with MSA during the marine period. c) Hourly averages of the estimated fraction of nss-SO₄ attributed to anthropogenic sources. Inset pie charts depict anthropogenic and biogenic contributions to nss-SO₄ (left) and total inorganic NR-PM₁ (right) during the marine period. Mass loadings of nitrate and chloride comprise less than 2% of total inorganic aerosol

1045
1046
1047
1048
1049
1050
1051
1052
1053
1054
1055
1056
1057
1058
1059
1060
1061
1062
1063
1064
1065
1066
1067
1068
1069
1070
1071
1072

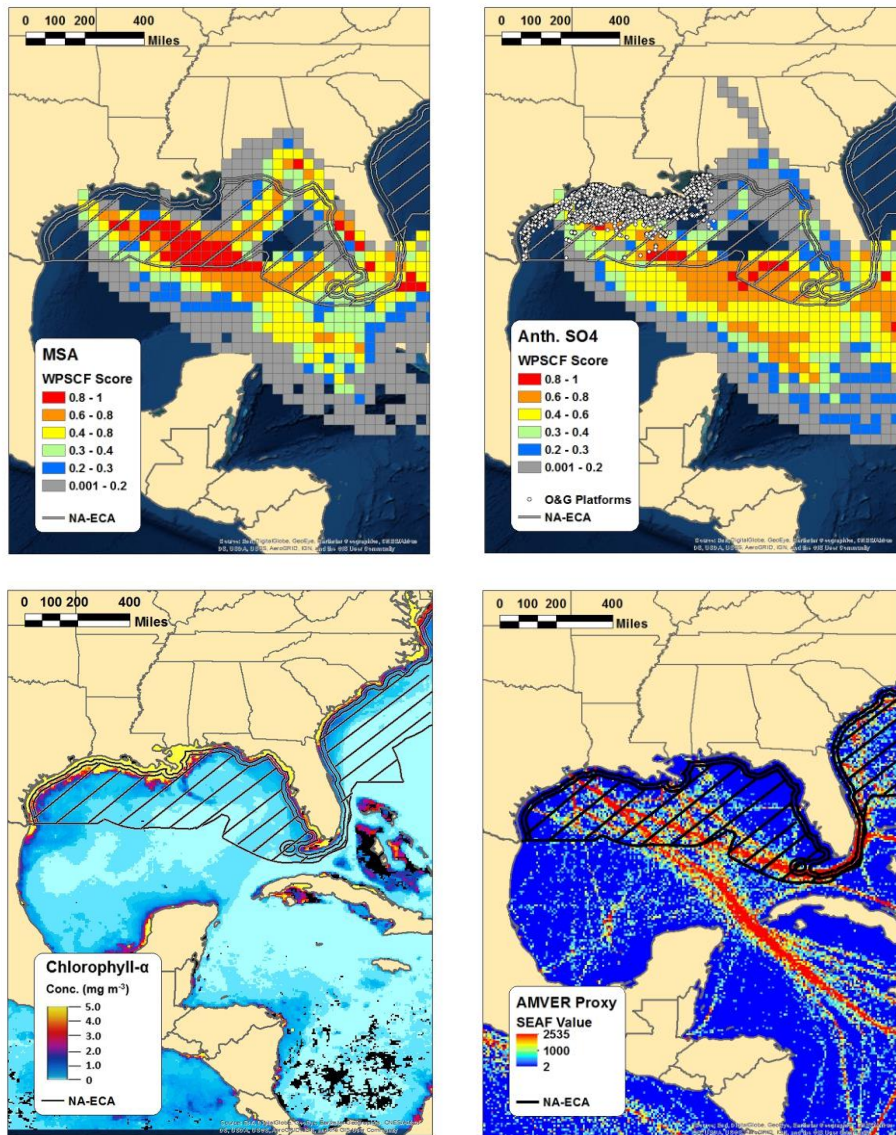


Figure 5: WPSFC plots of MSA (top-left) and anthropogenic nss-SO₄ (top-right) for the marine period of the study, along with the chlorophyll-a concentration observed by the NASA MODIS satellite (bottom-left) and AMVER shipping spatial proxy map (bottom-right). Warmer colors in the WPSFC grid cells indicate higher source probability. The color of each 0.1° x 0.1° grid cell in the AMVER map is based on the corresponding “shipping emissions allocation factor” (SEAF) value (Wang et al., 2008). The hatched region extending from the coasts in each panel represents the approximate area encompassed by the ECA. Note that the ECA boundary is narrowed on the southeastern coast of Florida due to proximity to the territorial waters of Cuba and the Bahamas.

1073
 1074
 1075
 1076
 1077
 1078
 1079
 1080
 1081
 1082
 1083
 1084
 1085
 1086
 1087
 1088
 1089
 1090
 1091
 1092
 1093
 1094
 1095
 1096
 1097
 1098
 1099
 1100

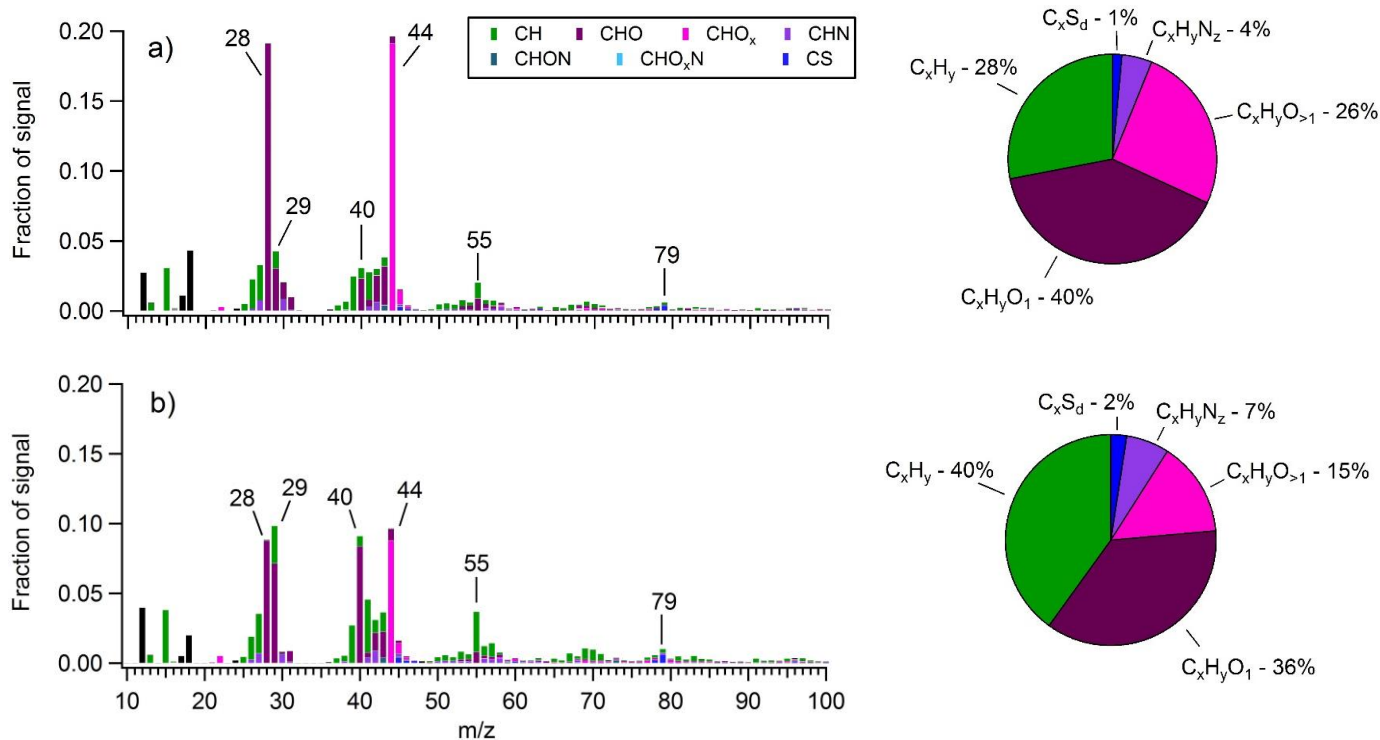


Figure 6: Average OA mass spectra measured during **a)** a period heavily influenced by shipping emissions (5/30/2016) and **b)** the “marine-biogenic” period when air masses traveled within the ECA for nearly their entire 5-day history. The overall organic fragment composition measured during each period is shown in the corresponding pie charts.

1101
1102
1103
1104
1105
1106
1107
1108
1109
1110
1111
1112
1113
1114
1115
1116
1117
1118
1119
1120
1121
1122
1123
1124
1125
1126
1127
1128

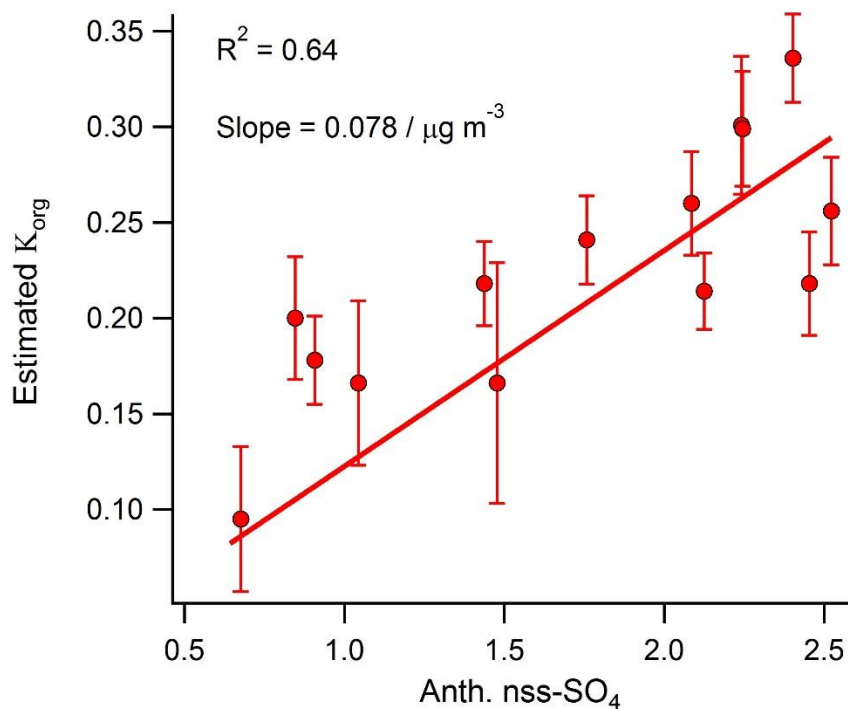


Figure 7: Correlation between daily-averaged anthropogenic nss-SO₄ and the OA hygroscopicity factor calculated using the method developed by Duplissy et al. (2011).

1129
1130
1131
1132
1133
1134
1135
1136
1137
1138
1139
1140
1141
1142
1143
1144
1145
1146
1147
1148
1149
1150
1151
1152
1153
1154
1155
1156

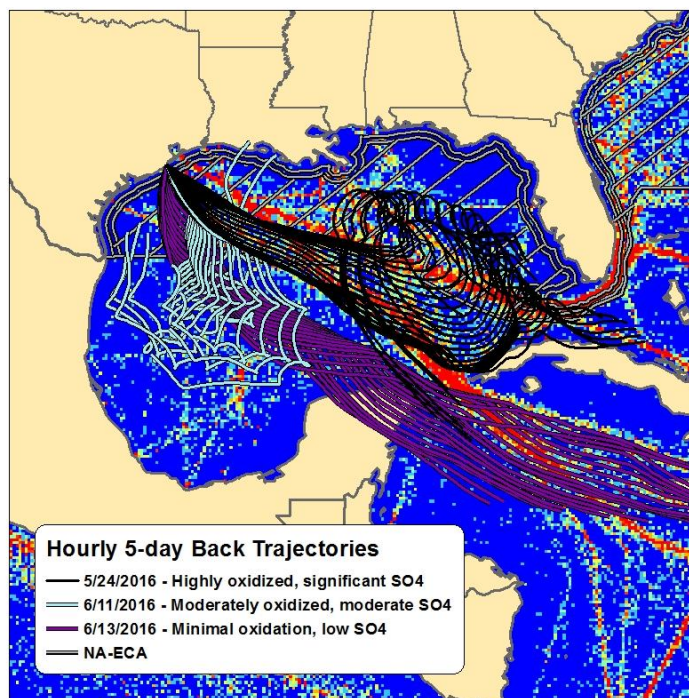
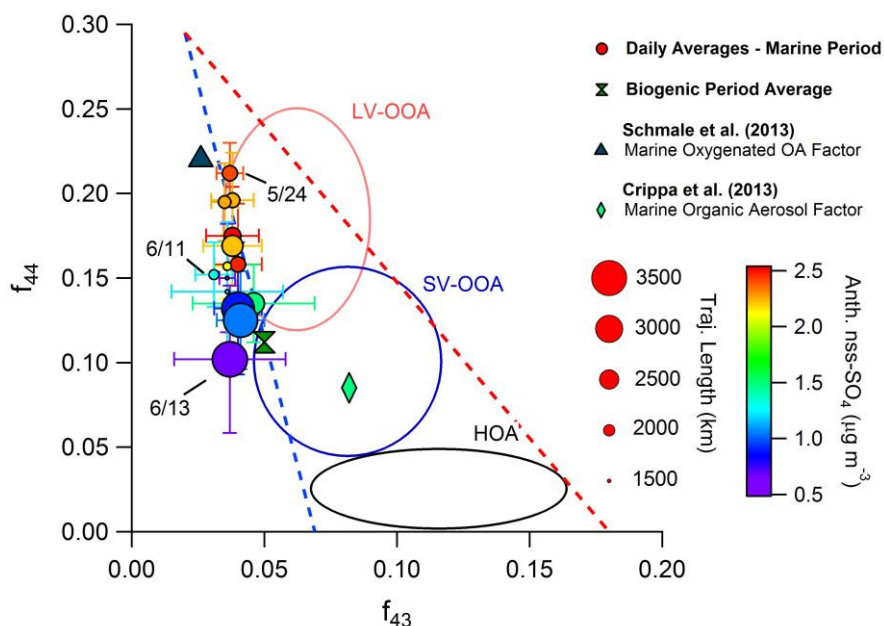


Figure 8: (Top) The $f_{44}:f_{43}$ diagram highlighting different influences on OA oxidation state during the marine period. Circles represent daily average values and bars indicate standard deviations. Periods with HOA mass loadings greater than twice the median value during the marine period were removed from the analysis. Two additional values from published marine studies are shown as a reference. (Bottom) Map of Gulf of Mexico showing hourly 5-day back trajectories calculated for each of the three days identified in the $f_{44}:f_{43}$ diagram. The AMVER shipping emissions spatial proxy map (Wang et al., 2008) is shown for reference. The hatched region extending from the coasts represents the approximate area encompassed by the ECA. Note that the ECA boundary is narrowed on the southeastern coast of Florida due to proximity to the territorial waters of Cuba and the Bahamas.

1157
1158
1159
1160
1161
1162
1163
1164
1165
1166
1167
1168
1169
1170
1171
1172
1173
1174
1175
1176
1177
1178
1179
1180
1181
1182
1183
1184

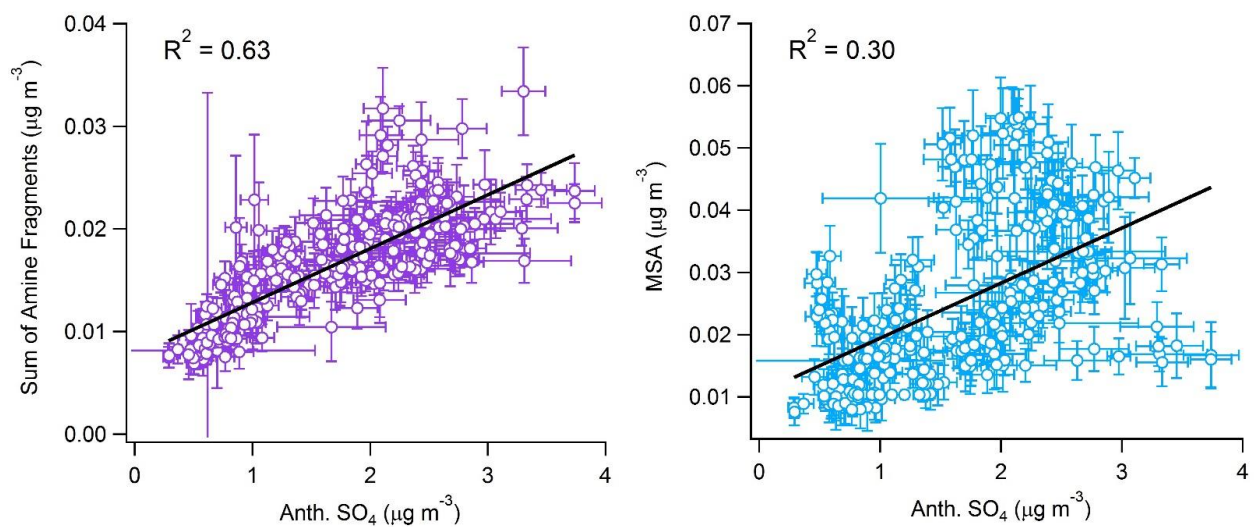


Figure 9: Observed correlation between anthropogenic nss- SO_4 and (left) the sum of measured alkyl amine fragments and (right) MSA.

1185
1186
1187
1188
1189
1190
1191
1192
1193
1194
1195
1196
1197
1198
1199
1200
1201
1202
1203
1204
1205
1206
1207
1208
1209
1210
1211
1212

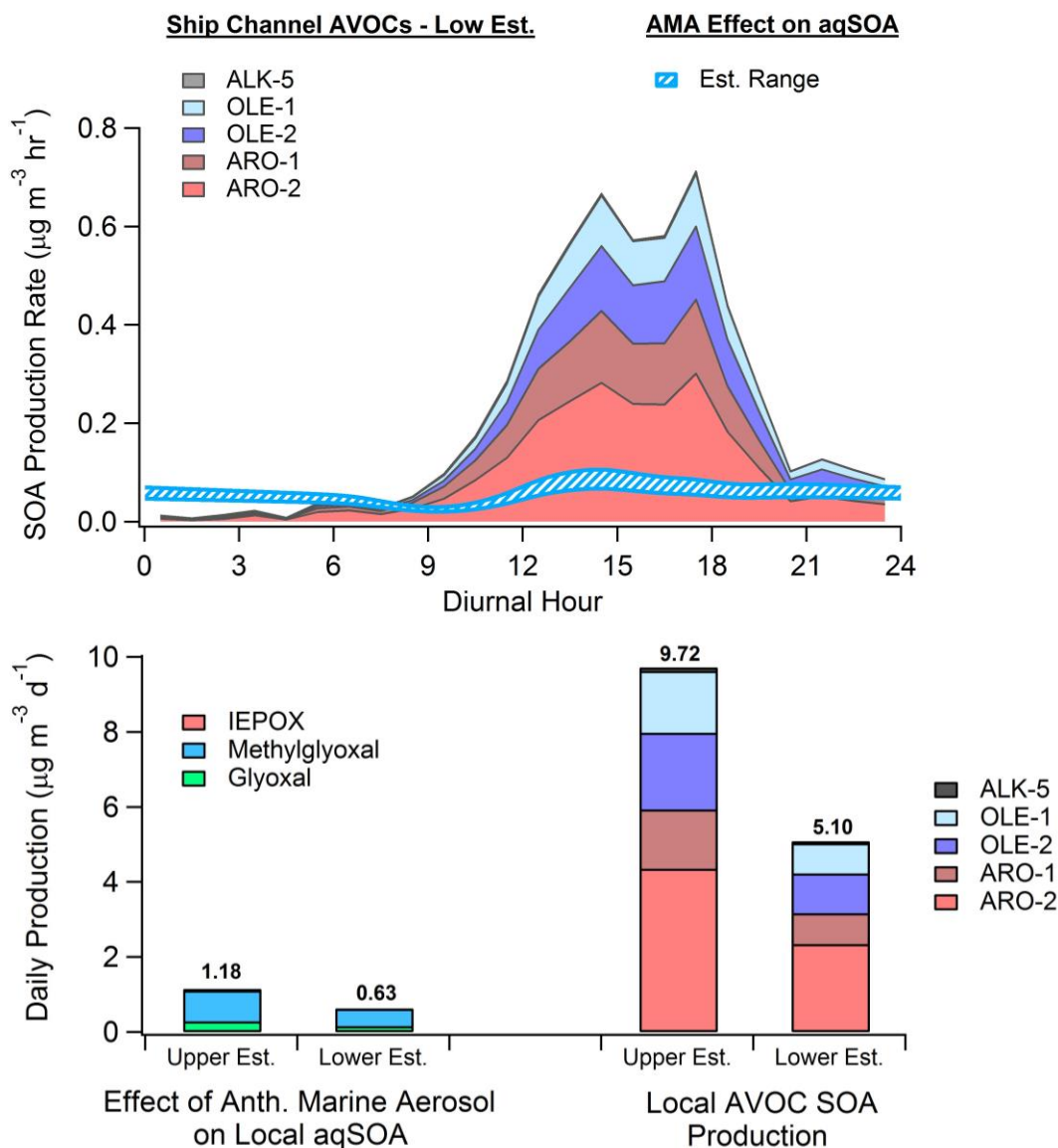


Figure 10: (Top) Diurnal SOA production rate calculated from anthropogenic VOCs (low estimate) measured by monitors in the HSC (filled) and the modeled-estimated production rate from WSOGs (glyoxal, methylglyoxal, IEPOX) attributable to the effect of anthropogenic marine aerosol (AMA) (hatched). (Bottom) Total daily SOA production from WSOGs (upper and lower estimates) and HSC AVOCs (upper and lower estimates). WSOG aqSOA production is characterized by individual species. Note that IEPOX production is negligible. AVOC SOA production is characterized by lumped VOC species defined in Tsimpidi et al. (2010). These species are further described in the SI. Upper and lower estimates of AVOC SOA production are based on the assumed background OA mass loading, as described in the SI. High-NO_x product yields were used for both AVOC estimates.

1213
1214
1215
1216
1217
1218
1219
1220
1221
1222
1223
1224
1225
1226
1227
1228
1229
1230
1231
1232
1233
1234
1235
1236
1237
1238
1239
1240
1241
1242
1243
1244
1245
1246
1247
1248
1249
1250
1251
1252
1253
1254
1255
1256
1257

References

- 1) Agrawal, H., Eden, R., Zhang, X., Fine, P. M., Katzenstein, A., Miller, J. W., Ospital, J., Teffera, S., and Cocker, D.: Primary particulate matter from ocean-going engines in the Southern California Air Basin, *Environ. Sci. Technol.*, 43, 5398-5402, doi: 10.1021/es8035016, 2009.
- 2) Agrawal, H., Welch, W. A., Miller, J. W., and Cocker, D. R.: Emission measurements from a crude oil tanker at sea, *Environ. Sci. Technol.*, 42, 7098-7103, doi: 10.1021/es703102y, 2008.
- 3) Aksoyoglu, S., Baltensperger, U., and Prevot, A. S.: Contribution of ship emissions to the concentration and deposition of air pollutants in Europe, *Atmos. Chem. Phys.*, 16, 1895-1906, doi: 10.5194/acp-16-1895-2016, 2016.
- 4) Bahreini, R., Ervens, B., Middlebrook, A.M., Warneke, C., de Gouw, J.A., DeCarlo, P.F., Jimenez, J.L., Brock, C.A., Neuman, J.A., Ryerson, T.B., Stark, H., Atlas, E., Brioude, J., Fried, A., Holloway, J.S., Peischl, J., Richter, D., Walega, J., Weibring, P., Wollny, A.G., and Fehsenfeld, F.C.: Organic aerosol formation in urban and industrial plumes near Houston and Dallas, Texas, *J. Geophys. Res.-Atmos.* 114, 17, doi: 10.1029/2008JD011493, 2009.
- 5) Bates, T.S., Quinn, P.K., Coffman, D., Schulz, K., Covert, D.S., Johnson, J.E., Williams, E.J., Lerner, B.M., Angevine, W.M., Tucker, S.C., Brewer, W.A., and Stohl, A.: Boundary layer aerosol chemistry during TexAQS/GoMACCS 2006: Insights into aerosol sources and transformation processes. *J. Geophys. Res.-Atmos.* 113, 18, doi: 10.1029/2008JD010023, 2008.
- 6) Bates, T. S., Quinn, P. K., Frossard, A. A., Russell, L. M., Hakala J., Petaja, T., Kulmala, M., Covert, D. S., Cappa, C. D., Li, S.-M., Hayden, K. L., Nuaaman, I., McLaren, R., Massoli, P., Canagaratna, M. R., Onasch, T. B., Sueper, D., Worsnop, D. R., and Keene, W. C.: Measurements of ocean derived aerosol off the coast of California, *J. Geophys. Res.*, 117, D00V15, doi: 10.1029/2012JD017588, 2012.
- 7) Bean, J. K., Faxon, C. B., Leong, Y. J., Wallace, H. W., Cevik, B. K., Ortiz, S., Canagaratna, M. R., Usenko, S., Sheesley, R. J., Griffin, R. J., and Hildebrandt, L: Composition and sources of particulate matter measured near Houston, TX; Anthropogenic-biogenic interactions, *Atmos.*, 5, 73, doi: 10.3390/atmos7050073, 2016.
- 8) Brown, S. S., Dubé, W. P., Bahreini, R., Middlebrook, A. M., Brock, C. A., Warneke, C., de Gouw, J. A., Washenfelder, R. A., Atlas, E., Peischl, J., Ryerson, T. B., Holloway, J. S., Schwarz, J. P., Spackman, R., Trainer, M., Parrish, D. D., Fehshenfeld, F. C., and Ravishankara, A. R.: Biogenic VOC oxidation and organic aerosol formation in an urban nocturnal boundary layer: aircraft vertical profiles in Houston, TX, *Atmos. Chem. Phys.*, 13, 11317–11337, doi: 10.5194/acp-13-11317-2013, 2013.

- 1258 9) Browning, L., Hartley, S., Bandemehr, A., Gathright, K., and Miller, W.: Demonstration of
1259 fuel switching on oceangoing vessels in the Gulf of Mexico, *J. Air. Waste Manag. Assoc.*,
1260 62(9):1093-1101, doi: 10.1080/10962247.2012.697974, 2012.
1261
- 1262 10) Budisulistiorini, S. H., Nenes, A., Carlton, A. G., Surratt, J. D., McNeill, V. F., and Pye, H.
1263 O. T.: Simulating aqueous phase isoprene epoxydiol (IEPOX) secondary organic aerosol
1264 production during the 2013 Southern Oxidant and Aerosol Study (SOAS), *Environ. Sci.*
1265 *Tech.*, 51, 5026-5034, doi: 10.1021/acs.est.6b05750, 2017.
1266
- 1267 11) Caiazzo, F., Ashok, A., Waitz, I. A., Yim, S. H. L., and Barrett, S. R. H.: Air pollution and
1268 early deaths in the United States: Part I: Quantifying the impact of major sectors in 2005,
1269 *Atmos. Environ.*, 79, 198-208, doi: 10.1016/j.atmosenv.2013.05.081, 2013.
1270
- 1271 12) Canagaratna, M. R., Jayne, J. T., Jimenez, J. L., Allan, J. D., Alfarra, M. R., Zhang, Q.,
1272 Onasch, T. B., Drewnick, F., Coe, H., Middlebrook, A., Delia, A., Williams, L. R., Trimborn,
1273 A. M., Northway, M. J., DeCarlo, P. F., Kolb, C. E., Davidovits, P., and Worsnop, D. R.:
1274 Chemical and microphysical characterization of ambient aerosols with the aerodyne aerosol
1275 mass spectrometer, *Mass Spectrom. Rev.*, 26, 185–222, doi: 10.1002/mas.20115, 2007.
1276
- 1277 13) Canagaratna, M. R., Jimenez, J. L., Kroll, J. H., Chen, Q., Kessler, S. H., Massoli, P.,
1278 Hildebrandt Ruiz, L., Fortner, E., Williams, L. R., Wilson, K. R., Surratt, J. D., Donahue, N.
1279 M., Jayne, J. T., and Worsnop, D. R.: Elemental ratio measurements of organic compounds
1280 using aerosol mass spectrometry: characterization, improved calibration, and implications,
1281 *Atmos. Chem. Phys.*, 15, 253-272, <https://doi.org/10.5194/acp-15-253-2015>, 2015.
1282
- 1283 14) Carlton, A. G. and Turpin, B. J.: Particle partitioning potential of organic compounds is
1284 highest in the Eastern U.S. and driven by anthropogenic water, *Atmos. Chem. Phys.*, 13,
1285 10203–10214, doi: 10.5194/acp-13-10203-2013, 2013.
1286
- 1287 15) Chang, R. Y.-W., Leck, C., Graus, M., Müller, M., Paatero, J., Burkhardt, J. F., Stohl, A., Orr,
1288 L. H., Hayden, K., Li, S.-M., Hansel, A., Tjernström, M., Leitch, W. R., and Abbatt, J. P.
1289 D.: Aerosol composition and sources in the central Arctic Ocean during ASCOS, *Atmos.*
1290 *Chem. Phys.*, 11, 10619–10636, doi: 10.5194/acp-11-10619-2011, 2011.
1291
- 1292 16) Chen, G., Huey, L. G., Trainer, M., Nicks, D., Corbett, J., Ryerson, T., Parrish, D., Neuman,
1293 J. A., Nowak, J., Tanner, D., Holloway, J., Brock, C., Crawford, J., Olson, J. R., Sullivan, A.,
1294 Weber, R., Schauffler, S., Donnelly, S., Atlas, E., Roberts, J., Flocke, F., Hubler, G., and
1295 Fehsenfeld, F.: An investigation of the chemistry of ship emission plumes during ITCT 2002,
1296 *J. Geophys. Res.*, 110, D10S90, doi: 10.1029/2004JD005236, 2005.
1297
- 1298 17) Chhabra, P. S., Flagan, R. C., and Seinfeld, J. H.: Elemental analysis of chamber organic
1299 aerosol using an aerodyne high-resolution aerosol mass spectrometer, *Atmos. Chem. Phys.*,
1300 10, 4111–4131, doi: 10.5194/acp-10-4111-2010, 2010.
1301
- 1302 18) Chhabra, P. S., Ng, N. L., Canagaratna, M. R., Corrigan, A. L., Russell, L. M., Worsnop, D.
1303 R., Flagan, R. C., and Seinfeld, J. H.: Elemental composition and oxidation of chamber
1304 organic aerosol, *Atmos. Chem. Phys.*, 11, 8827–8845, doi: 10.5194/acp-11-8827-2011, 2011.

- 1305
1306 19) Claeys, M. B., Wang, W., Vermeylen, R., Kourtchev, I., Chi, X., Farhat, Y.J., Surratt, D.,
1307 Gomez-Gonzalez, Y., Sciare, J., and Maenhaut, W.: Chemical characterization of marine
1308 aerosol at Amsterdam Island during the austral summer of 2006–2007, *J. Aero. Sci.*, 41(1),
1309 13–22, doi: 10.1016/j.jaerosci.2009.08.003, 2009.
1310
1311 20) Cleveland, M. J., Ziemba, L. D., Griffin, R. J., Dibb, J. E., Anderson C. H., Lefer, B., and
1312 Rappengluck, B.: Characterization of urban aerosol using aerosol mass spectrometry and
1313 proton nuclear magnetic resonance spectroscopy, *Atmos. Environ.*, 511-518, 54, doi:
1314 10.1016/j.atmosenv.2012.02.074, 2012.
1315
1316 21) Coakley, J. A., Jr., Bernstein, R. L., and Durkee, P. A.: Effect of ship-stack effluents on
1317 cloud reflectivity, *Science*, 237, 1020-1022, doi: 10.1126/science.237.4818.1020, 1987.
1318
1319 22) Coggon, M. M., Sorooshian, A., Wang, Z., Metcalf, A. R., Frossard, A. A., Lin, J. J., Craven,
1320 J. S., Nenes, A., Jonsson, H. H., Russell, L. M., Flagan, R. C., and Seinfeld, J. H.: Ship
1321 impacts on the marine atmosphere: insights into the contribution of shipping emissions to the
1322 properties of marine aerosol and clouds, *Atmos. Chem. Phys.*, 12, 8439–8458, doi:
1323 10.5194/acp-12-8439- 2012, 2012.
1324
1325 23) Coggon, M.M., Sorooshian, A., Wang, Z., Craven, J.S., Metcalf, A.R., Lin, J.J., Nenes, A.,
1326 Jonsson, H.H., Flagan, R.C., and Seinfeld, J.H.: Observations of continental biogenic impacts
1327 on marine aerosol and clouds off the coast of California. *J. Geophys. Res.* 119, 6724-6748,
1328 doi: 10.1002/2013JD021228, 2014.
1329
1330 24) Corbett, J.J., and Kohler, H.W.: Updated emissions from ocean shipping. *J. Geophys. Res.*,
1331 108. doi: 10.1029/2003JD003751, 2003.
1332
1333 25) Corbett, J. J., Winebrake, J. J., Green, E. H., Kasibhatla, P., Eyring, V., and Lauer, A.:
1334 Mortality from ship emissions: A global assessment, *Environ. Sci. Technol.*, 41, 8512–8518,
1335 doi: 10.1021/es071686z, 2007.
1336
1337 26) Crippa, M., Canonaco, F., Lanz, V. A., Äijälä, M., Allan, J. D., Carbone, S., Capes, G.,
1338 Ceburnis, D., Dall’Osto, M., Day, D. A., De-Carlo, P. F., Ehn, M., Eriksson, A., Freney, E.,
1339 Hildebrandt Ruiz, L., Hillamo, R., Jimenez, J. L., Junninen, H., Kiendler-Scharr, A.,
1340 Kortelainen, A.-M., Kulmala, M., Laaksonen, A., Mensah, A. A., Mohr, C., Nemitz, E.,
1341 O’Dowd, C., Ovadnevaite, J., Pandis, S. N., Petäjä, T., Poulain, L., Saarikoski, S., Sellegri,
1342 K., Swietlicki, E., Tiitta, P., Worsnop, D. R., Baltensperger, U., and Prévôt, A. S. H.: Organic
1343 aerosol components derived from 25 AMS data sets across Europe using a consistent ME-2
1344 based source apportionment approach, *Atmos. Chem. Phys.*, 14, 6159–6176, doi:
1345 10.5194/acp-14-6159-2014, 2014.
1346
1347 27) Crippa, M., El Haddad, I., Slowik, J. G., DeCarlo, P. F., Mohr, C., Heringa, M. F., Chirico,
1348 R., Marchand, N., Sciare, J., Baltensperger, U., and Prévôt, A. S. H.: Identification of marine
1349 and continental aerosol sources in Paris using high resolution aerosol mass spectrometry, *J.*
1350 *Geophys. Res.-Atmos.*, 118, 1950–1963, doi: 10.1002/jgrd.50151, 2013.

- 1351
1352 28) Czech, H., Stengel, B., Adam, T., Sklorz, M., Streibel, T., and Zimmerman, R.: A
1353 chemometric investigation of aromatic emission profiles from a marine engine in comparison
1354 with residential wood combustion and road traffic: Implications for source apportionment
1355 inside and outside sulphur emission control areas, *Atmos. Environ.*, 167 212-222, doi:
1356 10/1016/j.atmosenv.2017.08.022, 2017.
1357
- 1358 29) DeCarlo, P. F., Kimmel, J. R., Trimborn, A., Northway, M. J., Jayne, J. T., Aiken, A. C.,
1359 Gonin, M., Fuhrer, K., Horvath, T., Docherty, K. S., Worsnop, D. R., and Jimenez, J. L.:
1360 Field-deployable, high-resolution, time-of-flight aerosol mass spectrometer, *Anal. Chem.*, 78,
1361 8281–8289, doi: 10.1021/ac061249n, 2006.
1362
- 1363 30) Draxler, R. R., and G. D. Rolph: HYSPLIT (Hybrid Single-Particle Lagrangian Integrated
1364 Trajectory) Model, access via NOAA ARL READY Website, NOAA Air Resources
1365 Laboratory, Silver Spring, MD., 2003. Available at [http://](http://www.arl.noaa.gov/ready/hysplit4.html)
1366 www.arl.noaa.gov/ready/hysplit4.html.
1367
- 1368 31) Duplissy, J., DeCarlo, P. F., Dommen, J., Alfarra, M. R., Metzger, A., Barmapadimos, I.,
1369 Prevot, A. S. H., Weingartner, E., Tritscher, T., Gysel, M., Aiken, A. C., Jimenez, J. L.,
1370 Canagaratna, M. R., Worsnop, D. R., Collins, D. R., Tomlinson, J., and Baltensperger, U.:
1371 Relating hygroscopicity and composition of organic aerosol particulate matter, *Atmos.*
1372 *Chem. Phys.*, 11, 1155–1165, doi: 10.5194/acp-11-1155-2011, 2011.
1373
- 1374 32) Durkee, P. A., Noone, K. J., and Bluth, R. T.: The Monterey Area Ship Track Experiment, *J.*
1375 *Atmos. Sci.*, 57, 2523-2541, doi: 10.1175/1520-0469(2000)057<2523:TMASTE>2.0.CO;2,
1376 2000.
1377
- 1378 33) Ervens, B., Sorooshian, A., Lim, Y. B., and Turpin, B.: Key parameters controlling OH-
1379 initiated formation of secondary organic aerosol in the aqueous phase (aqSOA), *J. Geophys.*
1380 *Res. Atmos.*, 119, 3997-4016, doi: 10.1002/2013JD021021, 2014.
1381
- 1382 34) Ervens, B., Turpin, B. J., and Weber, R. J.: Secondary organic aerosol formation in cloud
1383 droplets and aqueous particles (aqSOA): a review of laboratory, field and model studies,
1384 *Atmos. Chem. Phys.*, 11, 11069–11102, doi: 10.5194/acp-11-11069-2011, 2011.
1385
- 1386 35) Eyring, V., H. W. Kohler, A. Lauer, and Lemper, B.: Emissions from international shipping:
1387 2. Impact of future technologies on scenarios until 2050, *J. Geophys. Res.*, 110, D17301, doi:
1388 10.1029/2004JD005620, 2005.
1389
- 1390 36) Eyring, V., Isaksen, I. S. A., Berntsen, T., Collins, W. J., Corbett, J. J., Endresen, O.,
1391 Grainger, R. G., Moldanova, J., Schlager, H., and Stevenson, D. S.: Transport impacts on
1392 atmosphere and climate: Shipping, *Atmos. Environ.*, 44, 4735–4771, doi:
1393 10.1016/j.atmosenv.2009.04.059, 2010.
1394
- 1395 37) Facchini, M. C., Decesari, S., Rinaldi, M., Carbone, C., Finessi, E., Mircea, M., Fuzzi, S.,
1396 Moretti, F., Tagliavini, E., Ceburnis, D., and O’Dowd, C. D.: Important source of marine

- 1397 secondary organic aerosol from biogenic amines, *Environ. Sci. Technol.*, 42, 9116–9121, doi:
1398 10.1021/es8018385, 2008.
1399
- 1400 38) Faloona, I.: Sulfur processing in the marine atmospheric boundary layer: A review and
1401 critical assessment of modeling uncertainties, *Atmos. Environ.*, 43, 2841-2854, doi:
1402 10.1016/j.atmosenv.2009.02.043, 2009.
1403
- 1404 39) Fountoukis, C. and Nenes, A.: ISORROPIA II: a computationally efficient thermodynamic
1405 equilibrium model for K^+ - Ca^{2+} - Mg^{2+} - NH_4^+ - Na^+ - SO_4^{2-} - NO_3^- - Cl^- - H_2O aerosols, *Atmos.*
1406 *Chem. Phys.*, 7, 4639-4659, <https://doi.org/10.5194/acp-7-4639-2007>, 2007.
1407
- 1408 40) Frossard, A. A., Russell, L. M., Burrows, S. M., Elliott, S. M., Bates, T. S., and Quinn, P. K.:
1409 Sources and composition of submicron organic mass in marine aerosol particles, *J. Geophys.*
1410 *Res.- Atmos.*, 119, 12977–13003, doi: 10.1002/2014JD021913, 2014.
1411
- 1412 41) Fu, T., Jacob, D. J., Wittrock, F., Burrows, J. P., Vrekoussis, M., and Henze, D. K.: Global
1413 budgets of atmospheric glyoxal and methylglyoxal, and implications for formation of
1414 secondary organic aerosols, *J. Geophys. Res. Atmos.*, 113, 15 303, doi:
1415 10.1029/2007JD009505, 2008.
1416
- 1417 42) Fu, P., Kawamura, K., and Miura, K.: Molecular characterization of marine organic aerosols
1418 collected during a round-the-world cruise, *J. Geophys. Res. Atmos.*, 116, D13, doi:
1419 10.1029/2011JD015604, 2011.
1420
- 1421 43) Gantt, B., Meskhidze, N., Facchini, M. C., Rinaldi, M., Ceburnis, D., and O'Dowd, C. D.:
1422 Wind speed dependent size-resolved parameterization for the organic mass fraction of sea
1423 spray aerosol, *Atmos. Chem. Phys.*, 11, 8777–8790, doi: 10.5194/acp-11-8777-2011, 2011.
1424
- 1425 44) Gantt, B. and Meskhidze, N.: The physical and chemical characteristics of marine primary
1426 organic aerosol: a review, *Atmos. Chem. Phys.*, 13, 3979-3996, [https://doi.org/10.5194/acp-](https://doi.org/10.5194/acp-13-3979-2013)
1427 [13-3979-2013](https://doi.org/10.5194/acp-13-3979-2013), 2013.
1428
- 1429 45) Gaston, C. J., Pratt, K. A., Qin, X., and Prather, K. A.: Real-time detection and mixing state
1430 of methanesulfonate in single particles at an inland urban location during a phytoplankton
1431 bloom, *Environ. Sci. Technol.*, 44, 1566–1572, doi: 10.1021/es902069d, 2010.
1432
- 1433 46) Ge, X., Zhang, Q., Sun, Y., Ruehl, C. R., and Setyan, A.: Effect of aqueous-phase processing
1434 on aerosol chemistry and size distributions in Fresno, California, during wintertime, *Environ.*
1435 *Chem.*, 9, 221–235. <http://dx.doi.org/10.1071/en11168>, 2012.
1436
- 1437 47) Guo, Q., Hu, M., Guo, S., Wu, Z., Hu, W., Peng, J., Hu, W., Wu, Y., Yuan, B., Zhang, Q.,
1438 and Song, Y.: The identification of source regions of black carbon at a receptor site off the
1439 eastern coast of China, *Atmos. Environ.*, 100, 78-84, doi: 10.1016/j.atmosenv.2014.10.053,
1440 2014.
1441

- 1442 48) Hayes, P. L., Carlton, A. G., Baker, K. R., Ahmadov, R., Washenfelder, R. A., Alvarez, S.,
1443 Rappenglück, B., Gilman, J. B., Kuster, W. C., de Gouw, J. A., Zotter, P., Prévôt, A. S. H.,
1444 Szidat, S., Kleindienst, T. E., Offenberg, J. H., Ma, P. K., and Jimenez, J. L.: Modeling the
1445 formation and aging of secondary organic aerosols in Los Angeles during CalNex 2010,
1446 *Atmos. Chem. Phys.*, 15, 5773-5801, <https://doi.org/10.5194/acp-15-5773-2015>, 2015.
1447
- 1448 49) Hayes, P. L., Ortega, A. M., Cubison, M. J., Froyd, K. D., Zhao, Y., Cliff, S. S., Hu, W. W.,
1449 Toohey, D. W., Flynn, J. H., Lefer, B. L., Grossberg, N., Alvarez, S., Rappenglück, B.,
1450 Taylor, J. W., Allan, J. D., Holloway, J. S., Gilman, J. B., Kuster, W. C., de Gouw, J. A.,
1451 Massoli, P., Zhang, X., Liu, J., Weber, R. J., Corrigan, A. L., Russell, L. M., Isaacman, G.,
1452 Worton, D. R., Kreisberg, N. M., Goldstein, A. H., Thalman, R., Waxman, E. M., Volkamer,
1453 R., Lin, Y. H., Surratt, J. D., Kleindienst, T. E., Offenberg, J. H., Dusanter, S., Griffith, S.,
1454 Stevens, P. S., Brioude, J., Angevine, W. M., and Jimenez, J. L.: Organic aerosol
1455 composition and sources in Pasadena, California, during the 2010 CalNex campaign, *J.*
1456 *Geophys. Res.-Atmos.*, 118, 9233–9257, doi: 10.1002/jgrd.50530, 2013.
1457
- 1458 50) Hildebrandt, L., Engelhart, G. J., Mohr, C., Kostenidou, E., Lanz, V. A., Bougiatioti, A.,
1459 DeCarlo, P. F., Prevot, A. S. H., Baltensperger, U., Mihalopoulos, N., Donahue, N. M., and
1460 Pandis, S. N.: Aged organic aerosol in the Eastern Mediterranean: the Finokalia Aerosol
1461 Measurement Experiment – 2008, *Atmos. Chem. Phys.*, 10, 4167-4186,
1462 <https://doi.org/10.5194/acp-10-4167-2010>, 2010.
1463
- 1464 51) Hildebrandt, L., Kostenidou, E., Lanz, V. A., Prevot, A. S. H., Baltensperger, U.,
1465 Mihalopoulos, N., Laaksonen, A., Donahue, N. M., and Pandis, S. N.: Sources and
1466 atmospheric processing of organic aerosol in the Mediterranean: insights from aerosol mass
1467 spectrometer factor analysis, *Atmos. Chem. Phys.*, 11, 12499-12515,
1468 <https://doi.org/10.5194/acp-11-12499-2011>, 2011.
1469
- 1470 52) Hopke, P.K., Barrie, L.A., Li, S.M., Cheng, M.D., Li, C., and Xie, Y.: Possible sources and
1471 preferred pathways for biogenic and non-sea-salt sulfur for the high arctic. *J. Geophys. Res.*
1472 *Atmos.* 100 (D8), 16595-16603, doi: 10.1029/95JD01712, 1995.
1473
- 1474 53) Huang, D. D., Li, Y. J., Lee, B. P., and Chan, C. K.: Analysis of organic sulfur compounds in
1475 atmospheric aerosols at the HKUST supersite in Hong Kong using HR-ToF-AMS, *Environ.*
1476 *Sci. Technol.*, 49, 3672–3679, doi: 10.1021/es5056269, 2015.
1477
- 1478 54) Huang, S., Poulain, L., Pinxteren, D. V., Pinxteren, M. V., Wu, Z., Herrmann, H., and
1479 Wiedensohler, A.: Latitudinal and seasonal distribution of particulate MSA over the Atlantic
1480 using a validated quantification method with HR-ToF-AMS, *Environ. Sci. Technol.*, 51, 418-
1481 426, doi: 10.1021/acs.est.6b03186, 2017.
1482
- 1483 55) Hynes, A.J., Wine, P.H., and Semmes, D.H.: Kinetics and mechanism of hydroxyl reactions
1484 with organic sulfide, *J. Phys. Chem.* 90, 4148-4156, doi: 10.1021/j100408a062, 1986.
1485
- 1486 56) IMO: International Shipping Facts and Figures – Information Resources on Trade, Safety,
1487 Security, Environment. International Maritime Organization, 2012.

1488
1489 57) Johansson, L., Jalkanen, J.-P., and Kukkonen, J.: Global assessment of shipping emissions in
1490 2015 on a high spatial and temporal resolution, *Atmos. Environ.*, 167, 403-415, doi:
1491 10.1016/j.atmosenv.2017.08.042, 2017.
1492
1493 58) Jung, J., Furutani, H., Uematsu, M., and Park, J.: Distributions of atmospheric non-sea-salt
1494 sulfate and methanesulfonic acid over the Pacific Ocean between 48°N and 55°S during
1495 summer, *Atmos. Environ.*, 99, 374-384, doi: 10.1016/j.atmosenv.2014.10.009, 2014.
1496
1497 59) Kasper, A., S. Aufdenblatten, A. Forss, M. Mohr, and Burtscher, H.: Particulate emissions
1498 from a low-speed marine diesel engine, *Aerosol Sci. Technol.*, 41, 24 – 32, doi:
1499 10.1080/02786820601055392, 2007.
1500
1501 60) Kerminen, V.-M., Aurela, M., Hillamo, R.E., and Virkkula, A.: Formation of particulate
1502 MSA: deductions from size distribution measurements in the Finnish Arctic. *Tellus*, 49B,
1503 159-171, doi: 10.3402/tellusb.v49i2.15959, 1997.
1504
1505 61) Kim, H. S., Kim, Y. H., and Song, C. H.: Ship-plume sulfur chemistry: ITCT 2K2 case study,
1506 *Sci. Tot. Environ.*, 450-451:178-87, doi:10.1016/j.scitotenv.2013.01.099, 2013.
1507
1508 62) Kim, H. S., Song, C. H., Park, R. S., Huey, G., and Ryu, J. Y.: Investigation of ship-plume
1509 chemistry using a newly-developed photochemical/dynamic ship-plume model, *Atmos.*
1510 *Chem. Phys.*, 9, 7531–7550, doi: 10.5194/acp-9-7531-2009, 2009.
1511
1512 63) Kotchenruther, R.: The effects of marine vessel fuel sulfur regulations on ambient PM_{2.5} at
1513 coastal and near coastal monitoring sites in the U.S., *Atmos. Environ.*, 151, 52-61, doi:
1514 10.1016/j.atmosenv.2016.12.012, 2016.
1515
1516 64) Lack, D. A., Corbett, J. J., Onasch, T., Lerner, B., Massoli, P., Quinn, P. K., Bates, T. S.,
1517 Covert, D. S., Coffman, D., Sierau, B., et al.: Particulate emissions from commercial
1518 shipping: Chemical, physical, and optical properties, *J. Geophys. Res.*, 114, D00F04, doi:
1519 10.1029/2008JD011300, 2009.
1520
1521 65) Lack, D. A., Cappa, C. D., Langridge, J., Bahreini, R., Buffaloe, G., Brock, C. A., Cerully,
1522 K., Hayden, K., Holloway, J. S., Lerner, B., Li, S. M., McLaren, R., Middlebrook, A.,
1523 Moore, R., Nenes, A., Nuaanman, I., Peischl, J., Perring, A., Quinn, P. K., Ryerson, T. B.,
1524 Schwarz, J. P., Spackman, J. R., and Williams, E. J.: Impact of fuel quality regulation and
1525 speed reductions on shipping emissions: Implications for climate and air quality, *Environ.*
1526 *Sci. Technol.*, 45, 9052–9060, doi: 10.1021/es2013424, 2011.
1527
1528 66) Lauer, A., Eyring, V., Hendricks, J., Jockel, P., and Lohmann, U.: Effects of oceangoing
1529 shipping on aerosols and clouds. *Atmos. Chem. Phys.* 7, 5061–5079, doi: 10.5194/acp-7-
1530 5061-2007, 2007.
1531
1532 67) Lawrence, M. G., and Crutzen, P. J.: Influence of NO_x emissions from ships on tropospheric
1533 photochemistry and climate, *Nature*, 402, 167-170, doi: 10.1038/46013, 1999.
1534

- 1535 68) Leong, Y. J., Sanchez, N. P., Wallace, H. W., Cevik, K., Hernandez, C. S., Han, Y., Flynn, J.
1536 H., Massoli, P., Floerchinger, C., Fortner E. C., Herndon, S., Bean, J. K., Hildebrandt Ruiz,
1537 L., Jeon, W., Choi, Y., Lefer, B., and Griffin, R. J.: Overview of surface measurements and
1538 spatial characterization of submicrometer particulate matter during the DISCOVER-AQ 2013
1539 campaign in Houston, *J. Air Waste Manage. Assoc.*, 28, 1-19, doi:
1540 10.1080/10962247.2017.1296502, 2017.
1541
- 1542 69) Li, J., Cleveland, M., Ziemba, L. D., Griffin, R. J., Barsanti, K. C., Pankow, J. F., Ying, Q.:
1543 Modeling regional secondary organic aerosol using the Master Chemical Mechanism, *Atmos.*
1544 *Environ.*, 102, 52-61, doi: 10.1016/j.atmosenv.2014.11.054, 2015.
1545
- 1546 70) Lin, C. T., Baker, A. R., Jickells, T. D., Kelly, S., and Lesworth, T.: An assessment of the
1547 significance of sulphate sources over the Atlantic Ocean based on sulphur isotope data,
1548 *Atmos. Environ.*, 62, 615-621, doi: 10.1016/j.atmosenv.2012.08.052, 2012.
1549
- 1550 71) Liu, H., Fu, M., Jin, X., Shang, Y., Shindell, D., Faluvegi, G., Shindell, C., and He, K.:
1551 Health and climate impacts of ocean-going vessels in East Asia, *Nat. Clim. Change Adv.*, 6,
1552 1037-1041, doi: 10.1038/nclimate3083, 2016.
1553
- 1554 72) McNeill, V. F.: Aqueous organic chemistry in the atmosphere: sources and chemical
1555 processing of organic aerosols, *Environ. Sci. Technol.*, 49, 1237-1244, doi:
1556 10.1021/es5043707, 2015.
1557
- 1558 73) Middlebrook, A. M., Bahreini, R., Jimenez, J. L., and Canagaratna, M. R.: Evaluation of
1559 composition-dependent collection efficiencies for the Aerodyne aerosol mass spectrometer
1560 using field data, *Aerosol. Sci. Technol.*, 46, 258-271, doi: 10.1080/02786826.2011.620041,
1561 2011.
1562
- 1563 74) Murphy, S. M., Sorooshian, A., Kroll, J. H., Ng, N. L., Chhabra, P., Tong, C., Surratt, J. D.,
1564 Knipping, E., Flagan, R. C., and Seinfeld, J. H.: Secondary aerosol formation from
1565 atmospheric reactions of aliphatic amines, *Atmos. Chem. Phys.*, 7, 2313-2337,
1566 <https://doi.org/10.5194/acp-7-2313-2007>, 2007.
1567
- 1568 75) Murphy, S. M., Agrawal, H., Sorooshian, A., Padro, L. T., Gates, H., Hersey, S., Welch, W.
1569 A., Jung, H., Miller, J. W., Cocker, D. R., Nenes, A., Jonsson, H. H., Flagan, R. C., and
1570 Seinfeld, J. H.: Comprehensive simultaneous shipboard and airborne characterization of
1571 exhaust from a modern container ship at sea, *Environ. Sci. Technol.*, 43, 4626-4640, doi:
1572 10.1021/es802413j, 2009.
1573
- 1574 76) Myriokefalitakis, S., Vignati, E., Tsigaridis, K., Papadimas, C., Sciare, J., Mihalopoulos, N.,
1575 Facchini, M. C., Rinaldi, M., Dentener, F. J., Ceburnis, D., Hatzianastasiou, N., O'Dowd, C.
1576 D., van Weele, M., and Kanakidou, M.: Global modelling of the oceanic source of organic
1577 aerosols, *Adv. Meteorol.*, 2010, 939171, doi: 10.1155/2010/939171, 2010.
1578
- 1579 77) Ng, N. L., Canagaratna, M. R., Zhang, Q., Jimenez, J. L., Tian, J., Ulbrich, I. M., Kroll, J. H.,
1580 Docherty, K. S., Chhabra, P. S., Bahreini, R., Murphy, S. M., Seinfeld, J. H., Hildebrandt, L.,
1581 Donahue, N. M., DeCarlo, P. F., Lanz, V. A., Prevot, A. S. H., Dinar, E., Rudich, Y., and

- 1582 Worsnop, D. R.: Organic aerosol components observed in Northern Hemispheric datasets
1583 from Aerosol Mass Spectrometry, *Atmos. Chem. Phys.*, 10, 4625–4641, doi: 10.5194/acp-10-
1584 4625-2010, 2010.
- 1585
- 1586 78) Nguyen, T. K. V., Zhang, Q., Jimenez, J. L., Pike, M., and Carlton, A. G.: Liquid water:
1587 ubiquitous contributor to aerosol mass, *Environ. Sci. Technol. Lett.*, 3, 257–263, doi:
1588 10.1021/acs.estlett.6b00167, 2016.
- 1589
- 1590 79) Nightingale, P. D., Liss, P. S., and Schlosser, P.: Measurements of air-sea gas transfer during
1591 an open ocean algal bloom, *J. Geophys. Res. Lett.*, 27, 2117–2120, doi:
1592 10.1029/2000GL011541, 2000.
- 1593
- 1594 80) Ortega, A. M., Hayes, P. L., Peng, Z., Palm, B. B., Hu, W., Day, D. A., Li, R., Cubison, M.
1595 J., Brune, W. H., Graus, M., Warneke, C., Gilman, J. B., Kuster, W. C., de Gouw, J.,
1596 Gutiérrez-Montes, C., and Jimenez, J. L.: Real-time measurements of secondary organic
1597 aerosol formation and aging from ambient air in an oxidation flow reactor in the Los Angeles
1598 area, *Atmos. Chem. Phys.*, 16, 7411–7433, <https://doi.org/10.5194/acp-16-7411-2016>, 2016.
- 1599
- 1600 81) Ovadnevaite, J., O’Dowd, C., Dall’Osto, M., Ceburnis, D., Worsnop, D. R., and Berresheim,
1601 H.: Detecting high contributions of primary organic matter to marine aerosol: A case study,
1602 *Geophys. Res. Lett.*, 38, L02807, doi: 10.1029/2010GL046083, 2011.
- 1603
- 1604 82) Ovadnevaite, J., Ceburnis, D., Leinert, S., Dall’Osto, M., Canagaratna, M., O’Doherty, S.,
1605 Berresheim, H., and O’Dowd, C.: Submicron NE Atlantic marine aerosol chemical
1606 composition and abundance: Seasonal trends and air mass categorization, *J. Geophys. Res.*
1607 *Atmos.*, 119, 11850–11863, doi: 10.1002/2013JD021330, 2014.
- 1608
- 1609 83) Paatero, P., and Tapper, U.: Positive matrix factorization – A nonnegative factor model with
1610 optimal utilization of error-estimates of data values, *Environmetrics*, 5, 111–126, doi:
1611 10.1002/env.3170050203, 1994.
- 1612
- 1613 84) Peters, K., Stier, P., Quaas, J., and Grabl, H.: Aerosol indirect effects from shipping
1614 emissions: sensitivity studies with the global aerosol-climate model ECHAM-HAM, *Atmos.*
1615 *Chem. Phys.*, 12, 5985–6007, doi: 10.5194/acp-12-5985-2012, 2012
- 1616
- 1617 85) “Port Houston Statistics” Port Houston. <http://porthouston.com/portweb/about-us/statistics/>,
1618 Accessed August 9, 2017.
- 1619
- 1620 86) Raper, J. L., Kleb, M. M., Jacob, D. J., Davis, D., Newell, R. E., Fuelberg, H. E., Bendura, R.
1621 J., Hoell, J. M., and McNeal, R. J.: Pacific Exploratory Mission in the Tropical Pacific: PEM
1622 Tropics B, March–April 1999, *J. Geophys. Res.-Atmos.*, 106, 32401–32425, doi:
1623 10.1029/2000JD900833, 2001.
- 1624
- 1625 87) Ren, X., van Duin, D., Cazorla, M., Chen, S., Mao, J., Zhang, L., Brune, W. H., Flynn, J.,
1626 Grossberg, N., Lefer, B. L., Rappengluck, B., Wong, K. W., Tsai, C., Stutz, J., Dibb, J. E.,
1627 Jobson, B. T., Luke, W. T., and Kelley, P.: Atmospheric oxidation chemistry and ozone

- 1628 production: Results from SHARP 2009 in Houston, Texas, *J. Geophys. Res. Atmos.*, 118,
1629 5770-5780, doi: 10.1002/jgrd.50342, 2013.
- 1630
- 1631 88) Rinaldi, M., Decesari, S., Finessi, E., Giulianelli, L., Carbone, C., Fuzzi, S., O'Dowd, C. D.,
1632 Ceburnis, D., and Facchini, M. C.: Primary and secondary organic marine aerosol and
1633 oceanic biological activity: Recent results and new perspectives for future studies, *Adv.*
1634 *Meteorol.*, 2010, 310–682, doi: 10.1155/2010/310682, 2010.
- 1635
- 1636 89) Russell, L. M., Takahama, S., Liu, S., Hawkins, L. N., Covert, D. S., Quinn, P. K., and Bates,
1637 T. S.: Oxygenated fraction and mass of organic aerosol from direct emission and atmospheric
1638 processing measured on the R/V Ronald Brown during TexAQS/GoMACCS 2006, *J.*
1639 *Geophys. Res. Atmos.*, 114, D00F05, doi: 10.1029/2008JD011275, 2009.
- 1640
- 1641 90) Russell, L. M., Hawkins, L. N., Frossard, A. A., Quinn, P. K., and Bates, T. S.:
1642 Carbohydrate-like composition of submicron atmospheric particles and their production from
1643 ocean bubble bursting, *P. Natl. Acad. Sci. USA*, 107, 6652–6657, doi:
1644 10.1073/pnas.0908905107, 2010.
- 1645
- 1646 91) Saltzman, E. S., D. L. Savoie, R. G. Zika, and J. M. Prospero: Methane sulfonic acid in the
1647 marine atmosphere, *J. Geophys. Res.*, 88, 10,897–10,902, doi: 10.1029/JC088iC15p10897,
1648 1983.
- 1649
- 1650 92) Savoie, D. L., Arimoto, R., Keene, W. C., Prospero, J. M., Duce, R. A., and Galloway, J. N.:
1651 Marine biogenic and anthropogenic contributions to non-sea-salt sulfate in the marine
1652 boundary layer over the North Atlantic Ocean, *J. Geophys. Res.*, 107, 4356, doi:
1653 10.1029/2001JD000970, 2002.
- 1654
- 1655 93) Schmale, J., Schneider, J., Nemitz, E., Tang, Y. S., Dragosits, U., Blackall, T. D., Trathan, P.
1656 N., Phillips, G. J., Sutton, M., and Braban, C. F.: Sub-Antarctic marine aerosol: dominant
1657 contributions from biogenic sources, *Atmos. Chem. Phys.*, 13, 8669– 8694, doi: 10.5194/acp-
1658 13-8669-2013, 2013.
- 1659
- 1660 94) Schulze, B. C., Wallace, H. W., Flynn, J. H., Lefer, B. L., Erickson, M. H., Jobson, B. T.,
1661 Dusanter, S., Griffith, S. M., Hansen, R. F., Stevens, P. S., VanReken, T., and Griffin, R. J.:
1662 Differences in BVOC oxidation and SOA formation above and below the forest canopy,
1663 *Atmos. Chem. Phys.*, 17, 1805-1828, <https://doi.org/10.5194/acp-17-1805-2017>, 2017.
- 1664
- 1665 95) Setyan, A., Zhang, Q., Merkel, M., Knighton, W. B., Sun, Y., Song, C., Shilling, J. E.,
1666 Onasch, T. B., Herndon, S. C., Worsnop, D. R., Fast, J. D., Zaveri, R. A., Berg, L. K.,
1667 Wiedensohler, A., Flowers, B. A., Dubey, M. K., and Subramanian, R.: Characterization of
1668 submicron particles influenced by mixed biogenic and anthropogenic emissions using high-
1669 resolution aerosol mass spectrometry: results from CARES, *Atmos. Chem. Phys.*, 12, 8131-
1670 8156, doi: 10.5194/acp-12-8131-2012, 2012.
- 1671
- 1672 96) Shank, L. M., Howell, S., Clarke, A. D., Freitag, S., Brekhovskikh, V., Kapustin, V.,
1673 McNaughton, C., Campos, T., and Wood, R.: Organic matter and non-refractory aerosol over

1674 the remote Southeast Pacific: oceanic and combustion sources, *Atmos. Chem. Phys.*, 12, 557-
1675 576, <https://doi.org/10.5194/acp-12-557-2012>, 2012.
1676

1677 97) Shilling, J. E., Chen, Q., King, S. M., Rosenoern, T., Kroll, J. H., Worsnop, D. R., DeCarlo,
1678 P. F., Aiken, A. C., Sueper, D., Jimenez, J. L., and Martin, S. T.: Loading-dependent
1679 elemental composition of alpha-pinene SOA particles, *Atmos. Chem. Phys.*, 9, 771–782, doi:
1680 10.5194/acp-9-771-2009, 2009.
1681

1682 98) Sinreich, R., Coburn, S., Dix, B., and Volkamer, R.: Ship-based detection of glyoxal over the
1683 remote tropical Pacific Ocean, *Atmos. Chem. Phys.*, 10, 11359–11371, doi: 10.5194/acp-10-
1684 11359-2010, 2010.
1685

1686 99) Slowik, J. G., Stroud, C., Bottenheim, J. W., Brickell, P. C., Chang, R. Y.-W., Liggió, J.,
1687 Makar, P. A., Martin, R. V., Moran, M. D., Shantz, N. C., Sjostedt, S. J., van Donkelaar, A.,
1688 Vlasenko, A., Wiebe, H. A., Xia, A. G., Zhang, J., Leaitch, W. R., and Abbatt, J. P. D.:
1689 Characterization of a large biogenic secondary organic aerosol event from eastern Canadian
1690 forests, *Atmos. Chem. Phys.*, 10, 2825-2845, <https://doi.org/10.5194/acp-10-2825-2010>,
1691 2010.
1692

1693 100) Sorooshian, A., Padro, L. T., Nenes, A., Feingold, G., McComiskey, A., Hersey, S. P.,
1694 Gates, H., Jonsson, H. H., Miller, S. D., Stephens, G. L., Flagan, R. C., and Seinfeld, J. H.:
1695 On the link between ocean biota emissions, aerosol, and maritime clouds: Airborne, ground,
1696 and satellite measurements off the coast of California, *Global Biogeochem. Cy.*, 23, Gb4007,
1697 doi: 10.1029/2009gb003464, 2009.
1698

1699 101) Sorooshian, A., Crosbie, E., Maudlin, L. C., Youn, J. S., Wang, Z., Shingler, T., Ortega,
1700 A. M., Hersey, S., and Woods, R. K.: Surface and airborne measurements of organosulfur
1701 and methanesulfonate over the western United States and coastal areas, *J. Geophys. Res.*,
1702 120, 8535–8548, doi: 10.1002/2015JD023822, 2015a.
1703

1704 102) Sorooshian, A., Prabhakar, G., Jonsson, H., Woods, R. K., Flagan, R. C., and Seinfeld, J.
1705 H.: On the presence of giant particles downwind of ships in the marine boundary layer, 42,
1706 2024-2030, doi: 10.1002/2015GL063179, 2015b.
1707

1708 103) Sun, Y.-L., Zhang, Q., Schwab, J. J., Demerjian, K. L., Chen, W.-N., Bae, M.-S., Hung,
1709 H.-M., Hogrefe, O., Frank, B., Rattigan, O. V., and Lin, Y.-C.: Characterization of the
1710 sources and processes of organic and inorganic aerosols in New York city with a high-
1711 resolution time-of-flight aerosol mass spectrometer, *Atmos. Chem. Phys.*, 11, 1581-1602,
1712 <https://doi.org/10.5194/acp-11-1581-2011>, 2011.
1713

1714 104) Tao, I., Fairley, D., Kleeman, M. J., and Harley, R. A.: Effects of switching to lower
1715 sulfur marine fuel on air quality in the San Francisco Bay Area, *Environ. Sci. Technol.*, 47,
1716 10171-10178, doi: 10.1021/es401049x, 2013.
1717

- 1718 105) Tian, L., Ho, K.F., Louie, P.K.K., Qiu, H., Pun, V.C., Kan, H., Yu, I.T.S., Wong, T.W.:
1719 Shipping emissions associated with increased cardiovascular hospitalizations, *Atmos.*
1720 *Environ.*, 74, 320-325, doi: 10.1016/j.atmosenv.2013.04.014, 2013.
1721
- 1722 106) Tournadre, J.: Anthropogenic pressure on the open ocean: The growth of ship traffic
1723 revealed by altimeter analysis, *Geophys. Res. Lett.*, 41, 7924-7932, doi:
1724 10.1002/2014GL061786, 2014.
1725
- 1726 107) Tsimpidi, A. P., Karydis, V. A., Zavala, M., Lei, W., Molina, L., Ulbrich, I. M., Jimenez,
1727 J. L., and Pandis, S. N.: Evaluation of the volatility basis-set approach for the simulation of
1728 organic aerosol formation in the Mexico City metropolitan area, *Atmos. Chem. Phys.*, 10,
1729 525–546, doi: 10.5194/acp-10-525-2010, 2010.
1730
- 1731 108) Ulbrich, I. M., Canagaratna, M. R., Zhang, Q., Worsnop, D. R., and Jimenez, J. L.:
1732 Interpretation of organic components from Positive Matrix Factorization of aerosol mass
1733 spectrometric data, *Atmos. Chem. Phys.*, 9, 2891–2918, doi: 10.5194/acp-9-2891-2009,
1734 2009.
1735
- 1736 109) U.S. Army Corps of Engineers, Navigation Data Center, 2016: Waterborne Commerce
1737 Statistics Center, U.S. Waterborne Container Traffic in 2015 – 2003, available at:
1738 <http://www.navigationdatacenter.us/wcsc/containers.htm>, Accessed August 9, 2017
1739
- 1740 110) U.S. Environmental Protection Agency, 2010: Designation of North American Emission
1741 Control Area to Reduce Emissions from Ships: Regulatory Announcement. EPA-420-F-10-
1742 015.
1743
- 1744 111) U.S. Environmental Protection Agency, 2014: National Emissions Inventory (NEI) Data,
1745 available at: [https://www.epa.gov/air-emissions-inventories/2014-national-emissions-](https://www.epa.gov/air-emissions-inventories/2014-national-emissions-inventory-nei-data)
1746 [inventory-nei-data](https://www.epa.gov/air-emissions-inventories/2014-national-emissions-inventory-nei-data)., Accessed November 10, 2017
1747
- 1748 112) U.S. Environmental Protection Agency, 2017: Air Pollutants Emissions Trends Data,
1749 State Average Annual Emissions Trends, available at: [https://www.epa.gov/air-emissions-](https://www.epa.gov/air-emissions-inventories/air-pollutant-emissions-trends-data)
1750 [inventories/air-pollutant-emissions-trends-data](https://www.epa.gov/air-emissions-inventories/air-pollutant-emissions-trends-data)., Accessed November 10, 2017
1751
- 1752 113) Vaughan, S., Ingham, T., Whalley, L. K., Stone, D., Evans, M. J., Read, K. A., Lee, J. D.,
1753 Moller, S. J., Carpenter, L. J., Lewis, A. C., Fleming, Z. L., and Heard, D. E.: Seasonal
1754 observations of OH and HO₂ in the remote tropical marine boundary layer, *Atmos. Chem.*
1755 *Phys.*, 12, 2149–2172, doi: 10.5194/acp-12-2149- 2012, 2012.
1756
- 1757 114) Viana, M., Hammingh, P., Colette, A., Querol, X., Degraeuwe, B., de Vlieger, I., van
1758 Aardenne, J.: Impact of maritime transport emissions on coastal air quality in Europe, *Atmos.*
1759 *Environ.*, 90, 96–105, doi: 10.1016/j.atmosenv.2014.03.046, 2014.
1760
- 1761 115) Vutukuru, S., and Dabdub, D.: Modeling the effects of ship emissions on coastal air
1762 quality: A case study of southern California, *Atmos. Environ.*, 42, 3751-3764, doi:
1763 10.1016/j.atmosenv.2007.12.073, 2008.
1764

- 1765 116) Wallace, H. W., Sanchez, N. P., Flynn, J. H., Erickson, M. H., Lefer, B. L., and Griffin,
1766 R. J.: Source apportionment of particulate matter and trace gases near a major refinery near
1767 the Houston Ship Channel, *Atmos. Env.*, 173, 16-29, doi: 10.1016/j.atmosenv.2017.10.049,
1768 2018.
1769
- 1770 117) Wan, Z., Zhu, M., Chen, S., and Sperling, D.: Pollution: three steps to a green shipping
1771 industry. *Nature*, 530, 275-277, doi: 10.1038/530275a, 2016.
1772
- 1773 118) Wang, C., Corbett, J. J., and Firestone, J.: Improving spatial representation of global ship
1774 emissions inventories, *Environ. Sci. Tech.*, 42, 193-199, doi: 10.1021/es0700799, 2008.
1775
- 1776 119) Wilson, D., Billings, R., Chang, R., Enoch, S., Do, B., Perez, H., and Sellers, J.: Year
1777 2014 Gulfwide Emissions Inventory Study, U.S. Department of the Interior, Bureau of Ocean
1778 Energy Management, accessed at: [https://www.boem.gov/2014-Gulfwide-Emission-
1779 Inventory/](https://www.boem.gov/2014-Gulfwide-Emission-Inventory/), 2017
- 1780
- 1781 120) Wong, J. P. S., Lee, A. K. Y., and Abbatt, J. P. D: Impacts of sulfate seed acidity and
1782 water content on isoprene secondary organic aerosol formation, *Environ. Sci. Tech.*, 49,
1783 13215-13221, doi: 10.1021/acs.est.5b02686, 2015.
1784
- 1785 121) Wood, E. C., Canagaratna, M. R., Herndon, S. C., Onasch, T. B., Kolb, C. E., Worsnop,
1786 D. R., Kroll, J. H., Knighton, W. B., Seila, R., Zavala, M., Molina, L. T., DeCarlo, P. F.,
1787 Jimenez, J. L., Weinheimer, A. J., Knapp, D. J., Jobson, B. T., Stutz, J., Kuster, W. C., and
1788 Williams, E. J.: Investigation of the correlation between odd oxygen and secondary organic
1789 aerosol in Mexico City and Houston, *Atmos. Chem. Phys.*, 10, 8947–8968, doi: 10.5194/acp-
1790 10-8947-2010, 2010.
1791
- 1792 122) Wozniak, A. S., Willoughby, A. S., Gurganus, S. C., and Hatcher, P. G.: Distinguishing
1793 molecular characteristics of aerosol water soluble organic matter from the 2011 trans-North
1794 Atlantic US GEOTRACES cruise, *Atmos. Chem. Phys.*, 14, 8419-8434, doi: 10.5194/acp-14-
1795 8419-2014, 2014.
1796
- 1797 123) Ying, Q., Li, J., and Kota, S. H.: Significant contributions of isoprene to summertime
1798 secondary organic aerosol in eastern United States, *Environ. Sci. Tech.*, 49, 7834-7842, doi:
1799 10.1021/acs.est.5b02514, 2015.
1800
- 1801 124) Youn, J.-S., Crosbie, E., Maudlin, L. C., Wang, Z., and Sorooshian, A.: Dimethylamine
1802 as a major alkyl amine species in particles and cloud water: Observations in semi-arid and
1803 coastal regions, *Atmos. Environ.*, 122, 250–258, doi: 10.1016/j.atmosenv.2015.09.061, 2015.
1804
- 1805 125) Zetterdahl, M., Salo, K., Fridell, E., and Sjoblom, J.: Impact of aromatic concentration in
1806 marine fuels on particle emissions, *J. Mar. Sci. App.*, 16, 3, 352-361, doi: 10.1007/s11804-
1807 017-1417-7, 2017.
1808

- 1809 126) Zhao, M., Zhang, Y., Ma, W., Fu, Q., Yang, X., Li, C., Zhou, B., Yu, Q., and Chen, L:
1810 Characteristics and ship traffic source identification of air pollutants in China's largest port,
1811 Atmos. Environ., 64, 277-286, doi: 10.1016/j.atmosenv.2012.10.007, 2012.
1812
- 1813 127) Zhu, L., Huang, X., Shi, H., Cai, X., and Song, Y.: Transport pathways and potential
1814 sources of PM₁₀ in Beijing, Atmos. Environ. 45 (3), 594-604, doi:
1815 10.1016/j.atmosenv.2010.10.040, 2011.
1816
- 1817 128) Zorn, S. R., Drewnick, F., Schott, M., Hoffmann, T., and Borrmann, S.: Characterization
1818 of the South Atlantic marine boundary layer aerosol using an aerodyne aerosol mass
1819 spectrometer, Atmos. Chem. Phys., 8, 4711–4728, doi: 10.5194/acp-8-4711- 2008, 2008.